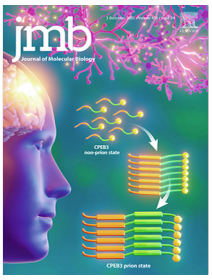

Cholesterol-Mediated Clustering of the HIV Fusion Protein gp41 in Lipid Bilayers

Nhi Tran [1], Younghoon Oh [2], Madeleine Sutherland [1], Qiang Cui [2,3,4*] and Mei Hong [1*]

*1 - **Department of Chemistry,** Massachusetts Institute of Technology, 170 Albany Street, Cambridge, MA 02139, United States*
*2 - **Department of Chemistry,** Boston University, 590 Commonwealth Avenue, Boston, MA 02215, United States*
*3 - **Department of Physics,** Boston University, 590 Commonwealth Avenue, Boston, MA 02215, United States*
*4 - **Department of Biomedical Engineering,** Boston University, 590 Commonwealth Avenue, Boston, MA 02215, United States*

Correspondence to Qiang Cui and Mei Hong: Department of Chemistry, Boston University, 590 Commonwealth Avenue, Boston, MA 02215, United States (Q. Cui); Department of Chemistry, Massachusetts Institute of Technology, 170 Albany Street, Cambridge, MA 02139, United States (M. Hong). *meihong@mit.edu (Q. Cui), qiangcui@bu.edu (M. Hong), @MeiHongLab (M. Hong)*
https://doi.org/10.1016/j.jmb.2021.167345
Edited by Ichio Shimada

Abstract

The envelope glycoprotein (Env) of the human immunodeficient virus (HIV-1) is known to cluster on the viral membrane surface to attach to target cells and cause membrane fusion for HIV-1 infection. However, the molecular structural mechanisms that drive Env clustering remain opaque. Here, we use solid-state NMR spectroscopy and molecular dynamics (MD) simulations to investigate nanometer-scale clustering of the membrane-proximal external region (MPER) and transmembrane domain (TMD) of gp41, the fusion protein component of Env. Using ^{19}F solid-state NMR experiments of mixed fluorinated peptides, we show that MPER-TMD trimers form clusters with interdigitated MPER helices in cholesterol-containing membranes. Inter-trimer ^{19}F-^{19}F cross peaks, which are indicative of spatial contacts within ~2 nm, are observed in cholesterol-rich virus-mimetic membranes but are suppressed in cholesterol-free model membranes. Water-peptide and lipid-peptide cross peaks in 2D ^{1}H-^{19}F correlation spectra indicate that the MPER is well embedded in model phosphocholine membranes but is more exposed to the surface of the virus-mimetic membrane. These experimental results are reproduced in coarse-grained and atomistic molecular dynamics simulations, which suggest that the effects of cholesterol on gp41 clustering is likely via indirect modulation of the MPER orientation. Cholesterol binding to the helix-turn-helix region of the MPER-TMD causes a parallel orientation of the MPER with the membrane surface, thus allowing MPERs of neighboring trimers to interact with each other to cause clustering. These solid-state NMR data and molecular dynamics simulations suggest that MPER and cholesterol cooperatively govern the clustering of gp41 trimers during virus-cell membrane fusion.

Introduction

The partitioning and clustering of eukaryotic membrane proteins to raft-like lipid domains play important roles in cellular signaling, vesicle trafficking, and cytoskeleton organization.[1–4] For example, intracellular membrane fusion between different organelles is accomplished by multiple SNARE proteins, which are clustered at the fusion site with the help of specific lipids.[5–7] In enveloped

viruses, clustering of viral membrane proteins to raft-like lipid domains is implicated in the lifecycle, entry, and infectivity of the viruses.[8,9] HIV-1 entry into cells is mediated by the surface envelope glycoprotein Env, which consists of trimeric assemblies of gp120 and gp41 heterodimers.[10] Following attachment of gp120 to cell-surface receptors, gp41 undergoes large conformational changes to fuse the target cell membrane with the virus envelope. However, each HIV-1 particle contains only 7 to 14 copies of Env, in contrast to other enveloped viruses such as alphaviruses and influenza, which contain many more entry proteins.[11,12] It has long been hypothesized that the low copy number of the HIV-1 entry protein may be compensated by a local clustering of the Env to accomplish the necessary membrane curvature for virus-cell fusion. Indeed, super-resolution microscopy and electron tomography data have captured Env clusters on the surface of the HIV-1 envelope and during virus-cell membrane fusion,[13–15] and this clustering correlates with HIV-1 infectivity.

While the existence of Env clustering has been demonstrated by microscopy data, the molecular mechanism of this clustering is not yet well understood. So far, Env clustering has been investigated largely in terms of Env interaction with other HIV-1 proteins and with host cell receptors. In immature and non-infectious HIV-1 particles, the structural polyprotein Gag interacts with Env through the cytoplasmic tail (CT) of gp41. Disassembly of the Gag lattice during HIV-1 maturation allows Env diffusion in the lipid envelope to form clusters that engage with cell surface receptors.[14,15] The gp41 CT also interacts with cholesterol, which may promote Env clustering to the cholesterol-rich domains of the lipid membrane.[16] Despite the role of the CT in HIV-1 maturation, CT-truncated Env may still be able to cluster in the membrane, since immature HIV-1 particles containing CT-truncated Env have been shown to have partial entry capability.[14,17,18] This observation suggests that alternative domains in gp41 may play important roles in Env clustering, independent of the cytoplasmic tail.

Gp41 contains a highly conserved membrane-proximal external region (MPER) immediately N-terminal to the transmembrane domain (TMD). This MPER forms an amphipathic α-helix on the surface of the lipid membrane,[19,20] and is required for viral membrane fusion. Biochemical studies showed that MPER peptides are able to destabilize lipid membranes and play a role in mediating lipid mixing during membrane fusion.[21] Analysis of ^{1}H and ^{13}C chemical shifts of POPC in the absence and presence of cholesterol and a pentapeptide of the MPER domain suggested that cholesterol promotes the insertion of this pentapeptide into the lipid membrane, and the peptide in turn sequesters cholesterol.[22] Fluorescence microscopy data showed that the MPER preferentially partitions into cholesterol-rich lipid domains.[23] Very recently, solid-state NMR data and MD simulations found that cholesterol molecules bind to the MPER-TMD peptides in lipid bilayers.[24] Together, these results suggest that cholesterol, which is required for HIV-1 infectivity,[25–28] might recruit MPER to raft-like lipid domains, in doing so causing clustering of the Env trimers.

Here we directly investigate the nanometer-scale separation of MPER-TMD trimers in lipid bilayers using 2D ^{19}F solid-state NMR experiments and molecular dynamics simulations. We prepared membrane samples with peptide/lipid molar ratios (P/L) of 1:10–1:32. At these peptide concentrations, previous ^{19}F spin-counting experiments showed that the MPER-TMD peptides are fully trimerized.[19] But whether the trimers cluster in space was not known. We now show that multiple MPER-TMD trimers indeed self-associate on the nanometer scale, and we provide direct experimental evidence for the dependence of this clustering on membrane cholesterol as well as constraints on the geometry of the clustered trimers.

Materials and Methods

Synthesis and purification of isotopically labeled gp41 MPER-TMD

The MPER-TMD peptide used in this study corresponds to residues 661–704 of HIV-1 clade D gp41. The amino acid sequence is ^{661}LELDKWASLW NWFNITNWLW YIRLFISIVG GLVGLRIVFA VLSI^{704}. This sequence is similar to the peptide used in our recent study of gp41 interaction with cholesterol,[24] except that we replaced M687 with Ser to prevent oxidation during peptide cleavage. Four fluorinated peptides were synthesized, each containing a single fluorinated residue at 4-CF_3-F673, 5-^{19}F-W670, 5-^{19}F-W666, and 4-CF_3-F663 (Table 1). For the 4-CF_3-F673 labeled peptide, ^{13}C, ^{15}N-labeled L684 was also incorporated. For the 4-CF_3-F663 labeled peptide, U-^{13}C, ^{15}N-labeled I675 and L679 were also incorporated. These ^{13}C, ^{15}N labeled residues serve to verify the secondary structure of the peptide. The 5-^{19}F-W670 labeled peptide and 4-CF_3-F673 peptide were mixed in a 1:1 molar ratio to produce membrane samples 1 – 4. The 5-^{19}F-W666 labeled peptide and 4-CF_3-F663 labeled peptide were mixed in a 1:1 molar ratio to produce samples 5 and 6.

These MPER-TMD peptides were synthesized on a custom-built fast-flow peptide synthesizer[29] using Fmoc solid-phase peptide synthesis protocols. Synthesis proceeded at 70 °C, with N,N-dimethylformamide (DMF) and the deprotection solution (25% piperidine) delivered at 20 ml/min. About 100 mg H-rink amide ChemMatrix resin with a loading of 0.5 mmol/g was swelled in the reaction vessel with DMF for 5 min. Fmoc-protected amino

Table 1 HIV gp41 MPER-TMD peptides and membrane samples used in this study.

Mixed peptide 1:

661 670 680 690 700
LELDKWASL WNWFNITNWL WYIRLFISIV GGLVGLRIVF AVLSI
LELDKWASL WNWFNITNWL WYIRLFISIV GGLVGLRIVF AVLSI

Membrane Samples	Peptide : Lipid : Chol molar ratio	Membrane composition
1	1 : 30 : 13	$VMS^{cluster}$
2	1 : 32 : 0	DMPC
3	1 : 10 : 4.5	VMS
4	1 : 32 : 0	POPE

Mixed peptide 2:

661 670 680 690 700
LEFDKWASL WNWFNITNWL WYIRLFISIV GGLVGLRIVF AVLSI
LEFDKWASL WNWFNITNWL WYIRLFISIV GGLVGLRIVF AVLSI

Membrane Samples	Peptide : Lipid : Chol molar ratio	Membrane composition
5	1 : 30 : 13	$VMS^{cluster}$
6	1 : 32 : 0	DMPC

acids were activated with 1-[Bis(dimethylamino)methylene]-1H-1,2,3-triazolo[4,5-b]pyridinium 3-oxide hexafluoro-phosphate (HATU) and N, N-Diisopropylethylamine (DIEA) prior to coupling with resin. The synthesis scale was 0.05 mmol, and ten-fold excess of unlabeled amino acids and four-fold excess of isotopically labeled amino acids were singly and triply coupled, respectively, using a coupling time of 50 and 70 s. The peptide was cleaved from the resin with TFA/phenol/H_2O/TIPS (88:5:5:2 v/v) for 3 h at room temperature. The resin was then filtered off and the crude peptide was precipitated and washed three times with chilled diethyl ether. The crude peptide was dried under vacuum overnight at room temperature.

Crude gp41 peptide was dissolved in trifluoroethanol (TFE) and purified by preparative reverse-phase HPLC using an organic solvent mixture/H_2O gradient. Solvent pumps A and B delivered 25:75 v/v acetonitrile: isopropanol in channel A and water in channel B at 15 ml/min. An isocratic gradient (5% A) was applied for one column volume (CV), followed by an initial linear gradient (5–60% A) over four CVs, and a final linear gradient (60–100% A) over 9 CVs. MALDI-MS was used to validate the peptide purity, with the measured masses showing good agreement with the calculated masses. The total yield of the peptide after purification was 15–20 mg (~8%).

Membrane sample preparation

The gp41(661–704) peptides were reconstituted into virus-mimetic phospholipid membranes ($VMS^{cluster}$ and VMS), which consists of 1-palmitoyl-2-oleyl-sn-glycerol-3-phosphocholine (POPC), 1-palmitoyl-2-oleoyl-sn-glycero-3-phosphoethanolamine (POPE), 1-palmitoyl-2-oleoyl-sn-glycero-3-phospho-L-serine (POPS), sphingomyelin (SM), and cholesterol (chol). The POPC:POPE:POPS:SM:chol molar ratios are 15:20:15:20:30 for the $VMS^{cluster}$ membrane and 30:15:15:10:30 for the VMS membrane. The $VMS^{cluster}$ membrane was designed to mimic the lipid compositions of the HIV envelope,[30,31] whereas the VMS membrane is more similar to the plasma membrane lipid composition. Two membrane samples (samples 1 and 5) were prepared with the $VMS^{cluster}$ membrane, where the peptide: (total phospholipid and SM): chol molar ratio (P/L/C) was 1:30:13 (Table 1). Control samples (samples 2 and 6) were prepared with the same peptides reconstituted in DMPC membranes at a P/L/C ratio of 1:32:0. Comparisons between samples 1 and 2 and between samples 5 and 6 allow us to investigate how the complex virus-mimetic membrane affects MPER-TMD trimer association. A VMS membrane sample (sample 3) with a higher P/L ratio of 1:10 was prepared to serve as a positive control for clustering, whereas a POPE sample (sample 4) with a P/L ratio of 1:32 further explores the impact of lipids on MPER-TMD clustering.

Phospholipids and SM were dissolved in chloroform and cholesterol was dissolved in a chloroform/methanol mixture. The peptides were dissolved in TFE and mixed with the lipid solution. The organic solvent was removed under nitrogen gas until a thin, dried lipid/peptide film was formed. This film was resuspended in HEPES buffer (10 mM HEPES, pH 7.5, 1 mM EDTA, 0.1 mM NaN_3) and subjected to ten freeze–thaw cycles between liquid nitrogen and a 45 °C water bath to form homogenous multilamellar vesicles. The proteoliposome solution was dialyzed against the buffer (pH 7.5) for 2.5 days with five buffer changes to remove residual TFE. The proteoliposomes were spun at 55,000 rpm using a Beckman SW60T rotor at 4 °C for 17 hours to obtain membrane pellets. The pellets were incubated in a desiccator until they reached a

hydration level of ~40 wt% water and were then spun into magic-angle spinning (MAS) rotors for solid-state NMR experiments. Most membrane samples contained ~8 mg peptide, 30–40 mg lipids, and ~30 mg water. The high-concentration VMS sample (sample 3) contained ~5 mg peptide, ~10 mg lipids, and ~10 mg water.

Solid-state NMR spectroscopy

Solid-state NMR spectra were measured on a Bruker AVANCE III HD spectrometer at 9.4 T (400 MHz ^{1}H Larmor frequency) using a 4 mm HFX MAS probe. ^{19}F chemical shifts were externally referenced to the ^{19}F signal of Teflon at −122 ppm on the $CFCl_3$ scale. ^{13}C chemical shifts were externally referenced to the $^{13}C\alpha$ signal of glycine at 43.65 ppm on the tetramethylsilane scale. Typical radiofrequency (rf) field strengths were 62.5 kHz for ^{19}F and ^{13}C pulses, and 50–62.5 kHz for ^{1}H decoupling using the two-pulse phase-modulated (TPPM) sequence.[32] 1D ^{19}F cross-polarization (CP) spectra were measured at 303–243 K under 10 kHz MAS.

2D ^{19}F-^{19}F correlation spectra were measured with a CORD[33] mixing time of 500 ms to investigate intermolecular contacts between MPER-TMD trimers (Table 2). To freeze protein motion, we measured most of these spectra at 243 K, except for the VMS sample (sample 3), which was measured at 238 K. The MAS frequencies were 10.0 and 10.332 kHz. For 2D spectra measured under 10.332 kHz MAS, the indirect dimension was rotor-synchronized to remove spinning sidebands and hence increase spectral sensitivity. The spectral width of 10.332 kHz corresponds to a ^{19}F chemical shift range of 27.5 ppm. The ^{19}F carrier frequency was set to −68 ppm for these experiments, thus the 5-^{19}F-W670 and 5-^{19}F-W666 peaks at −125 ppm are folded to −70 ppm in the indirect dimension, whereas the CF_3 signal of F673 and F663 appears at its true isotropic chemical shift of −62 ppm.

2D ^{1}H-^{19}F heteronuclear correlation (HETCOR) spectra with 100 ms ^{1}H spin diffusion were measured to investigate the depth of insertion of the fluorinated MPER residues.[34,35] For the DMPC membrane samples 2 and 6, the HETCOR spectra were measured at 290 K to reduce protein motion and enable efficient ^{1}H-^{19}F cross polarization. For the $VMS^{cluster}$ membrane samples 1 and 5, the HETCOR spectra were measured at 275 K to reach similar ^{1}H linewidths for the lipid CH_2 resonances at 1.2 and 1.3 ppm as the DMPC samples. In this way, we ensure that the $VMS^{cluster}$ and DMPC membranes have similar lipid chain dynamics and hence similar ^{1}H spin diffusion coefficients. At these temperatures, a ^{1}H T_2 filter of 0.2 ms was sufficient to remove all protein ^{1}H magnetization, thus ensuring that only lipid and water protons act as the ^{1}H magnetization source. Following ^{1}H chemical shift evolution, a ^{1}H mixing period of 100 ms was used to transfer the ^{1}H magnetization of lipids and water to the protein through chemical exchange and spin diffusion.[36,37] Cross-peak intensities between the lipid protons and protein fluorines, and between water protons and protein fluorines, indicate whether the fluorinated residues are well inserted into the membrane or reside on the membrane surface.

Molecular dynamics simulations

To probe the effect of cholesterol on the conformation and association of gp41 trimers, we conducted coarse-grained (CG) and all-atom molecular dynamics simulations. Most of the discussions in the main text center on all-atom simulations, whereas the CG simulation details and results are summarized in the SI (Figures S1 and S2).

Three different membrane models were used in the simulations, including the $VMS^{cluster}$ membrane and the DMPC membrane used in the solid-state NMR experiments, and a $VMS^{cluster}$ membrane without cholesterol (Table 3). The $VMS^{cluster}$ membrane contains POPC, POPE, POPS, PSM, and cholesterol with molar ratios of 15:20:15:20:30. To further understand the effect of cholesterol, we also compare the simulation results for $VMS^{cluster}$ membranes with and without cholesterol. For each membrane composition, two models of the MPER-TMD trimer were analyzed: a single trimer and a dimer of trimers. The structural model of the single trimer was adopted from the recent solid-state NMR study (PDB: 6DLN),[19] whereas the initial positions of the trimers in the dimer-of-trimer model were obtained from CG simulations. As described in the SI, these CG simulations revealed spontaneous clustering of the MPER-TMD trimers into three distinct geometries (Figure S1). We then used all-atom simulations to further examine the dimer model that features the most extensive gp41-gp41 contacts and to probe the effects of cholesterol on trimer clustering.

In all-atom simulations of both single trimer and dimer-of-trimer models, the peptide:lipid molar ratio is lower than that in the solid-state NMR experiments in order to avoid self-association of the trimers through periodic boundary images. Since many solid-state NMR experiments were conducted at low temperatures, we conducted MD simulations at both 303 K and 280 K to better compare the simulations with the NMR results, as well as to probe the physiological relevance of the observed clustering.

Initial configurations for MD simulations were built using CHARMM-GUI.[38,39] The protein-lipid systems were solvated with a 22.5-Å thick water layer on each side of the lipid bilayer. The gp41 trimers were placed in the lipid bilayer in a single orientation, with all MPER motifs interacting with the same membrane leaflet, to mimic the situation in the virus membrane. The CHARMM36 force field[40,41] and

Table 2 Parameters of the solid-state NMR experiments on the gp41 MPER-TMD membrane samples.

Experiment	NMR Parameters	Experimental Time	Membrane Samples
rotor synchronized 2D FF CORD	B_0 = 9.4 T, T_{set} = 243 K, ν_{MAS} = 10.332 kHz, SWH1 = 10.332 kHz, SWH2 = 93.75 kHz, ^{19}F carrier frequency = -68 ppm, ns = 640, τ_{rd} = 1.7 s, $t_{1,max}$ = 1.65 ms, $t_{1,inc}$ = 96.78 µs, τ_{dwell} = 5.3 µs, τ_{acq} = 4.3 ms, τ_{HF}= 1 ms, τ_{CORD} = 500 ms, $\nu_{1H,acq}$ = 71.4 kHz	40 hrs each 80 hrs	1, 2, 5 6
2D FF CORD	B_0 = 9.4 T, T_{set} = 238–243 K, ν_{MAS} = 10.0 kHz, SWH1 = 75 kHz, SWH1 = 93.75 kHz, ^{19}F carrier frequency = -83.6 ppm, ns = 256–320, τ_{rd} = 2 s, $t_{1,max}$ = 0.7 ms, $t_{1,inc}$ = 13.31 µs, τ_{dwell} = 5.3 µs, τ_{acq} = 3.1 – 4.3 ms, τ_{HF} = 750 µs, τ_{CORD} = 500 ms, $\nu_{1H,acq}$ = 35–50 kHz	89 hrs 71 hrs	3 4
2D ^{1}H-^{19}F HETCOR with 100 ms ^{1}H spin diffusion	B_0 = 9.4 T, T_{set} (samples 1 and 5) = 275 K, T_{set} (samples 2 and 6) = 290 K, ν_{MAS} = 9 kHz, SWH1 = 5 kHz, SWH1 = 93.75 kHz, ^{19}F carrier frequency = -83.6 ppm, ns = 1024, τ_{rd} = 1.5 s, $t_{1,max}$ = 4.8 ms, $t_{1,inc}$ = 200 us, τ_{dwell} = 5.3 µs, τ_{acq} = 4.3 ms, τ_{HF} = 1 ms, T_2'-filter duration = 222 µs, τ_{mix} = 100 ms, $\nu_{1H,acq}$ = 35–62.5 kHz	22 hrs each 45 hrs 89 hrs	1, 2 5 6

Symbols: B_0 = magnetic field; T_{set} = thermocouple-reported bearing gas temperature; ν_{MAS} = MAS frequency; SWH1: spectral width of the ω_1 dimension of the 2D spectra; SWH2: spectral width of the ω_2 dimension of the 2D spectra; ns = number of scans per t_1 slice of the 2D spectra; τ_{rd} = recycle delay; $t_{1,max}$ = maximum t_1 evolution time; $t_{1,inc}$ = increment or dwell time for the t_1 evolution period; τ_{dwell} = dwell time during direct acquisition of the FID; τ_{acq} = maximum acquisition time during direct detection; τ_{HF} = ^{1}H-^{19}F cross polarization contact time; τ_{CORD} = CORD mixing time. $\nu_{1H,\ acq}$ = ^{1}H decoupling field strength during detection.

the TIP3P model[42] were used to describe protein-lipid mixture and water, respectively. Na^+ and Cl^- ions were introduced to neutralize the system and maintain a concentration of 150 mM. All systems were equilibrated for at least 300 ns with the Highly Mobile Membrane Mimetic (HMMM) model[43] to facilitate the re-distribution of membrane components around the protein. Three configurations from the HMMM simulation were randomly selected, then converted to full-chain lipid membrane systems using CHARMM-GUI[44] and equilibrated for another 100 ns. During HMMM and equilibration following the conversion to full-chain lipids, all heavy atoms of the proteins were subjected to weak restraints. The production runs were free of any restraints and lasted for at least 200 ns for each system and the initial configuration. To help verify the robustness of the observed trends, especially the impact of cholesterol on the association of gp41 trimers, we also conducted dimer-of-trimer simulations in DMPC and cholesterol-free $VMS^{cluster}$ membranes, by starting with the tight dimer structure obtained by the end of MD simulations of the $VMS^{cluster}$ membrane.

All HMMM, equilibration and production simulations were performed under constant pressure and temperature using the Parrinello-Rahman barostat[45] and Nosè-Hoover thermostat.[46,47] Bonds involving hydrogen atoms were constrained using the LINCS algorithm,[48] which enables an integration time step of 2 fs. All simulations were carried out using the GROMACS-2018.3 simulation package.[49]

Results

MPER-TMD trimers co-localize in cholesterol-containing membranes

To investigate whether the MPER-TMD trimers cluster on the nanometer scale in lipid bilayers, we employed 2D ^{19}F-^{19}F spin diffusion correlation experiments. ^{19}F spin diffusion is able to detect distances up to ~2 nm due to the high gyromagnetic ratio of the ^{19}F spin and the resulting strong dipolar couplings.[50,51] Thus, if the fluorinated MPER residues from different trimers approach each other to within ~2 nm, we should observe inter-trimer correlation peaks. Most membrane samples prepared in this study have a peptide monomer:lipid molar ratio of about 1:30 (Table 1). This peptide concentration was chosen to allow sufficient separation between the MPER-TMD trimers if they are homogeneously distributed in the membrane while still permitting enough sensitivity for the NMR experiments. To investigate whether peptide clustering depends on the lipid composition of the membrane, we compare MPER-TMD bound to a cholesterol-containing virus-mimetic membrane ($VMS^{cluster}$) versus the one-component DMPC and POPE membranes.

Table 3 Membrane compositions and simulation temperatures for the systems studied with all-atom molecular dynamics simulations.

Membrane Model	Peptide:Lipid:Chol mole ratios	gp41 model and simulation temperature	
		A single trimer	Dimer of trimers
$VMS^{cluster}$	1:70:30	303 K, 280 K	303 K, 280 K
$VMS^{cluster}$ without cholesterol	1:93:0	303 K, 280 K	303 K, 280 K
DMPC	1:87:0	303 K, 280 K	303 K, 280 K

To maximally ensure that the measured intermolecular ^{19}F-^{19}F distances are between different trimers rather than within each trimer, we placed fluorinated residues at the N-terminal end of the MPER in one pair of mixed labeled samples and in the middle of the MPER helix in the other pair of mixed labeled samples. The first mixed-labeled sample contains 5F-W666 and 4-CF_3-F663 while the second mixed-labeled sample contains 5-F-W670 and 4-CF_3-F673 (Figure 1, Table 1). Based on a recently reported solid-state NMR structural model of trimeric MPER-TMD in lipid bilayers,[19] the distance between W670 and F673 on different protomers within the same trimer is expected to be at least 3 nm, whereas the intermolecular F663 – W666 distance within the same trimer is expected to be at least 4 nm. These intra-trimer distances significantly exceed the measurable ^{19}F-^{19}F distance upper limit of ~2 nm.[50] Thus, we do not expect to detect intra-trimer distances from these fluorinated residues. This assumption will be tested by measuring the ^{19}F-^{19}F correlation spectra of MPER-TMD in different membranes. If the ^{19}F labels are not sufficiently separated within each trimer, then we expect to detect ^{19}F-^{19}F cross peaks for all membrane compositions instead of only some of the membranes.

The NMR structural model indicates that the overall MPER helix length is about 29 Å, measured from L661 Cα to W680 Cα (Figure 1) At the P/L ratio of ~1:30, each trimer is on average solvated by about 45 lipid molecules in each leaflet, which occupy an area of ~29 nm^2. We estimate that this should be sufficient to separate the trimers if they are homogeneously distributed in the membrane instead of inhomogeneously clustered. This hypothesis can again be tested by measuring 2D ^{19}F-^{19}F correlation spectra in different lipid membranes. If the peptide concentration at a P/L of 1:30 is too high and cause close approach of trimers in all membranes, then ^{19}F-^{19}F correlation signals will be detected for all membrane compositions instead of only some of the membranes.

Figure 2(a) shows the 1D ^{19}F CP spectra of the two mixed labeled samples in the $VMS^{cluster}$ membrane. The 4-CF_3-labeled Phe residues show isotropic chemical shifts of −62 ppm whereas the 5-^{19}F-labeled Trp residues show isotropic chemical shifts of about −125 ppm (Figure 2(a)). The high sensitivity of the trifluoromethyl ^{19}F NMR signal facilitates the detection of long-range cross peaks.[50] 2D ^{13}C–^{13}C correlation spectra (Figure 2 (b, c)) of L684, L679, and I675 in the MPER show α-helical chemical shifts, confirming the helical conformation of the peptides in these membranes.

Figure 3 shows the 500 ms 2D ^{19}F-^{19}F spin diffusion spectra of fluorinated MPER-TMD in $VMS^{cluster}$ and DMPC membranes. These 2D spectra were measured with rotor synchronization for the indirect dimension to increase the spectral sensitivity. The 5F-Trp chemical shifts appear at folded positions of −70 ppm in the indirect dimension of these 2D spectra. We observed clear correlation signals between W670 and F673 in the $VMS^{cluster}$ membrane, but the cross peaks are absent in the DMPC membrane (Figure 3(a, b)). This contrast shows that intra-trimer distances are indeed too long to be measured, moreover the MPER-TMD trimers approach each other in the

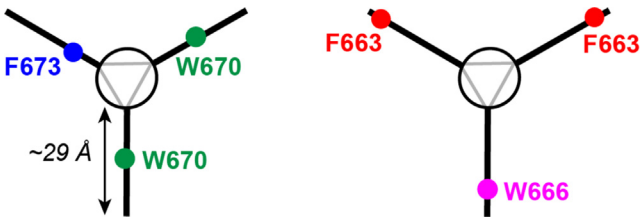

Figure 1. Schematic diagram of the dimension of MPER-TMD trimers and positions of fluorinated residues in the two mixed-labeled peptide samples. Each trimer, which has an MPER length of ~29 Å, is associated with a lipid area of ~29 nm^2 in each lipid leaflet at a P/L ratio of 1:30. If the trimers are uniformly distributed in the lipid membrane, then there is a sufficient number of lipid molecules to prevent interdigitation of two trimers.

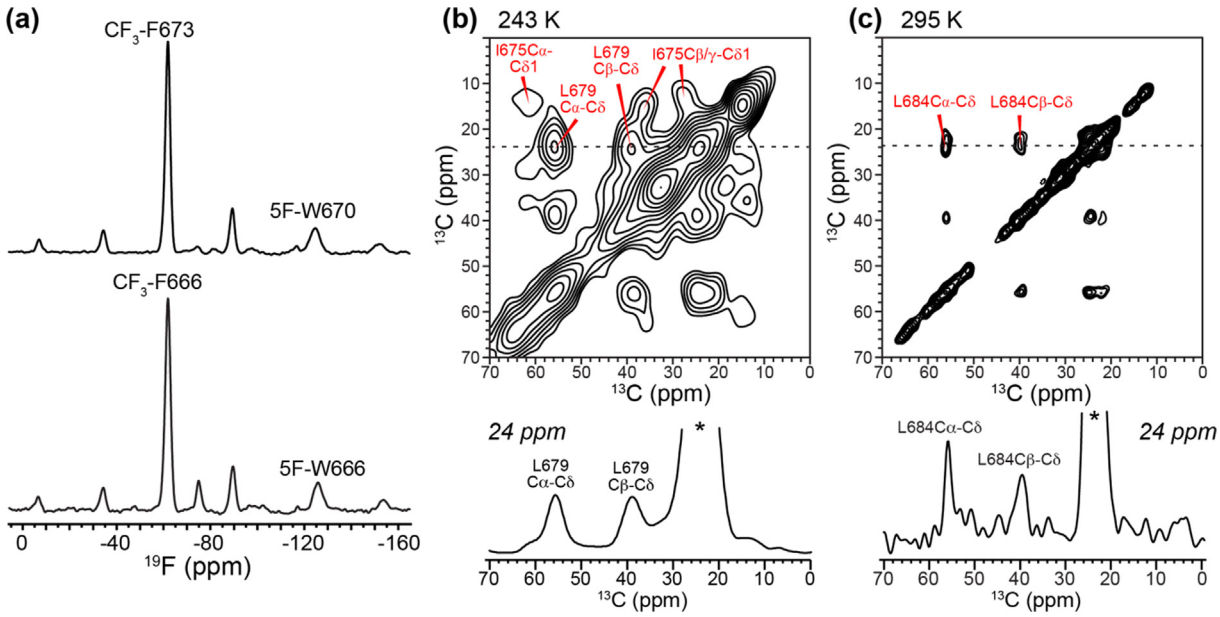

Figure 2. Characterization of the MPER-TMD conformation in the VMS^{cluster} membrane by ^{19}F and ^{13}C NMR. (a) 1D ^{19}F CP spectra of mixed CF_3-F673 and 5F-W670 labeled peptides (sample 1) and mixed CF_3-F663 and 5F-W666 labeled peptides (sample 5) in the VMS^{cluster} membrane. The spectra were measured at 243 K under 10.3 kHz MAS. (b) 2D ^{13}C–^{13}C correlation spectrum of I675 and L679 ^{13}C-labeled MPER-TMD in the VMS^{cluster} membrane (sample 5) at 243 K under 9 kHz MAS. The 24-ppm cross section is shown below, where the asterisk indicates the diagonal peak. (c) 2D ^{13}C–^{13}C correlation spectrum of L684 ^{13}C-labeled MPER-TMD in the VMS^{cluster} membrane (sample 1) at 295 K under 9 kHz MAS. The 24-ppm cross section is shown below.

cholesterol-containing VMS^{cluster} membrane. Similarly, correlation peaks between W666 and F663 are clearly observed in the VMS^{cluster} membrane but are much weaker in the DMPC membrane (Figure 3(c, d)). These results indicate that multiple MPER-TMD trimers cluster in the cholesterol-containing VMS^{cluster} membrane but not in the DMPC bilayer. We also measured 2D correlation spectra of POPE-bound peptide and observed no intermolecular cross peaks between W670 and F673 (Figure S3). As a positive control, 2D spectra of the peptide in the VMS^{cluster} membrane at a higher P/L ratio of 1:10 showed clear cross peaks between W670 and F673, as expected (Figure S3).

For the VMS^{cluster}-membrane bound sample, the cross-peak intensities are not symmetric: the magnetization transfer from 5F-Trp to CF_3-Phe (−70 ppm row) is higher than the reverse transfer from CF_3-Phe to 5F-Trp (−62 ppm row). We attribute these asymmetric cross peak intensities to the reduction of long-range ^{19}F-^{19}F dipolar coupling by the rotating CF_3 group, as previously shown for model compounds.[50] The close approach of W670 and F673 between two trimers, as well as the close approach of W666 and F663, suggest that two trimers interdigitate in the VMS^{cluster} membrane (Figure 5(a, b)), so that an MPER helix of one trimer packs in antiparallel with an MPER helix of a second trimer.

The MPER resides on the membrane surface in cholesterol-containing membranes

Since different MPER structural models have been proposed in micelles, bicelles and bilayers,[19,52–54] the MPER conformation is likely sensitive to the membrane environment. This suggests that clustering of the MPER-TMD trimers might perturb the MPER conformation, for example by squeezing the helix out of the membrane-water interface, whereas well separated and isolated trimers might allow the MPER to insert more deeply into the membrane. To test this hypothesis, we measured the depth of insertion of the MPER using 2D ^{1}H-^{19}F correlation experiments with ^{1}H spin diffusion.[34,35] Specifically, we measure the lipid-peptide and water-peptide ^{1}H-^{19}F cross peak intensities to probe the depth of insertion of the fluorinated residues.

Figure 4 shows 2D ^{1}H-^{19}F correlation spectra of the MPER-TMD peptides in VMS^{cluster} and DMPC membranes with 100 ms ^{1}H spin diffusion. The spectra were measured at 290 K for the DMPC samples and 275 K for the VMS^{cluster} samples to reach similar lipid chain dynamics and ^{1}H spin diffusion coefficients. This is verified by 1D ^{1}H MAS spectra of the two types of membrane samples, which show similar linewidths for the lipid CH_2, CH_3 and Hγ signals. At 290 K, fully hydrated pure DMPC membrane exists in the

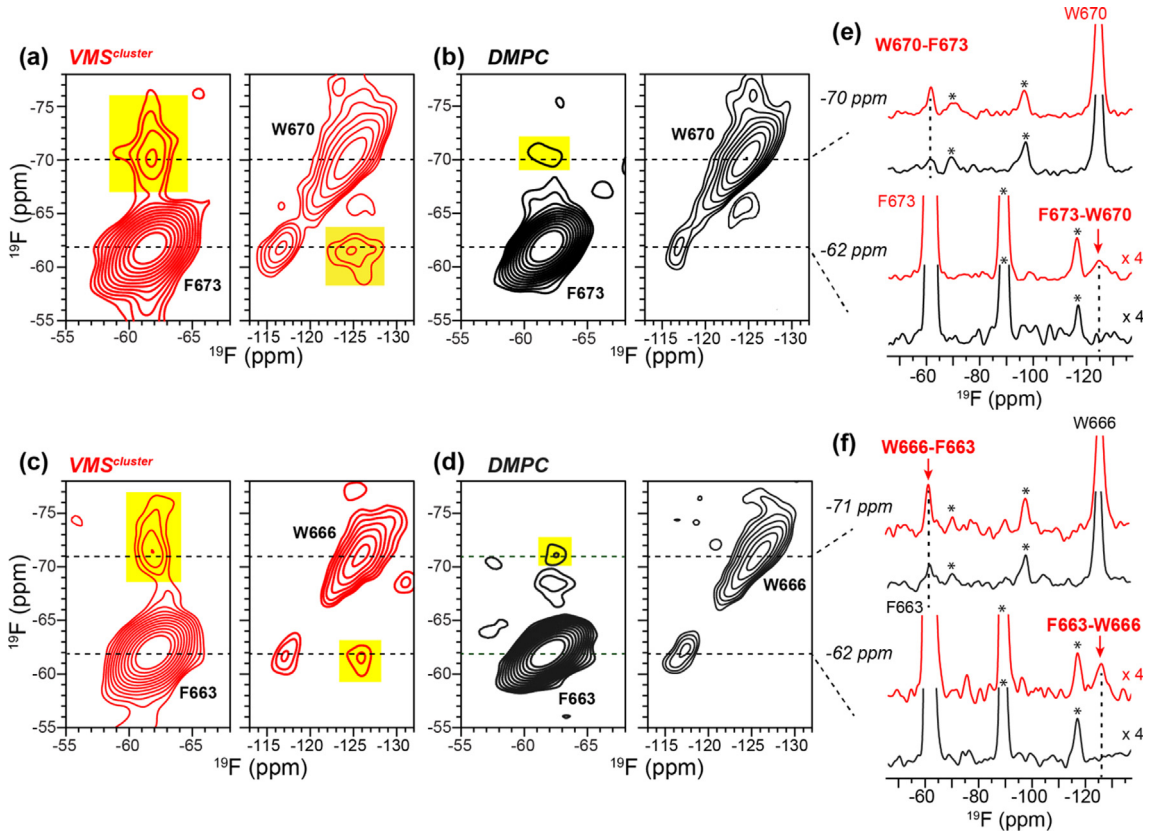

Figure 3. 500 ms 2D ^{19}F-^{19}F correlation spectra of mixed fluorinated gp41 trimers. (a) 2D spectrum of mixed 5F-W670 and CF_3-F673 labeled peptides in the VMS^{cluster} membrane at P/L = 1:30 (sample 1). (b) 2D spectrum of mixed 5F-W670 and CF_3-F673 labeled peptides in DMPC at P/L = 1:32 (sample 2). (c) 2D spectrum of mixed 5F-W666 and CF_3-F663 labeled peptides in the VMS^{cluster} membrane at P/L = 1:30 (sample 5). (d) 2D spectrum of 5F-W666 and CF_3-F663 mixed labeled peptide in DMPC at P/L = 1:32 (sample 6). Cross peaks are highlighted in yellow. (e) 1D ^{19}F cross sections of 5F-W670 and CF_3-F673 from the 2D spectra of the VMS^{cluster} sample and DMPC sample in (a) and (b). Asterisks indicate spinning sidebands. (f) 1D ^{19}F cross sections of W666 and F663 from the 2D spectra of the VMS^{cluster} sample and the DMPC sample in (c) and (d). All 2D spectra were measured at 243 K where protein motions were frozen.

rippled ($P_{\beta'}$) phase[55]; however, the peptide likely broadens the L_α-to-$P_{\beta'}$ phase transition. In both membranes, the CF_3-Phe and 5F-Trp signals show correlation peaks with the water and lipid CH_2 proton signals at 4.8 ppm and 1.2 ppm, respectively. Therefore, the MPER helix partitions to the membrane-water interface, in good agreement with the previous ^{13}C NMR spectra.[19] However, the relative intensities of the lipid and water cross peaks differ dramatically between the two membrane environments. The lipid-peptide cross peak intensities are 32–60% of the water-peptide cross-peak intensities in the DMPC membrane, but decrease to only 7–10% of the water-peptide cross peak intensities in the VMS^{cluster} membrane. This indicates that the MPER is much more deeply inserted into the DMPC bilayer than the VMS^{cluster} membrane. Moreover, in the DMPC membrane, the lipid cross peak intensities are high for C-terminal residues of the MPER but low for N-terminal residues, with an intensity trend of F673 > W670 > W666 > F663. This trend indicates that the MPER helix is tilted from the membrane plane, with the N-terminus more exposed to the aqueous solution while the C-terminus more immersed in the membrane (Figure 5 (c, d)). In contrast, in the VMS^{cluster} membrane, the four fluorinated residues show similarly weak lipid cross peak intensities, indicating that the MPER helix is parallel to the plane of the VMS^{cluster} membrane and is shallowly immersed.

Molecular dynamics capture trimer association and MPER orientation in cholesterol-containing membranes

To quantify the effect of the membrane composition on the orientation and depth of insertion of the MPER, we conducted all-atom molecular dynamics simulations, and evaluated the average Z positions of each amino acid

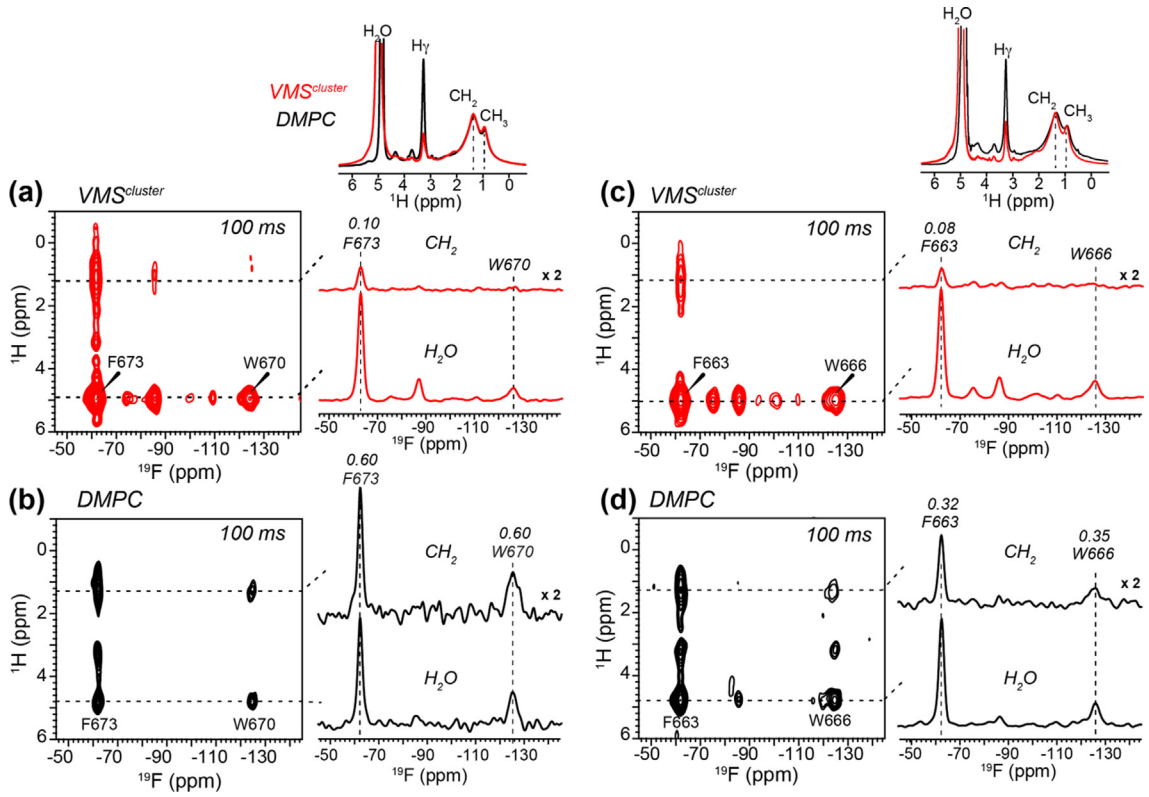

Figure 4. 2D ^{1}H-^{19}F HETCOR spectra for measuring the depth of insertion of MPER residues in different lipid membranes. (a) 2D spectrum of mixed 5F-W670 and CF_3-F673 labeled peptide in the VMS^{cluster} membrane at P/L = 1:30. (b) 2D spectrum of mixed 5F-W670 and CF_3-F673 labeled peptide in the DMPC membrane at P/L = 1:32. (c) 2D spectrum of mixed 5F-W666 and CF_3-F663 labeled peptide in the VMS^{cluster} membrane. (d) 2D spectrum of mixed 5F-W666 and CF_3-F663 labeled peptide in the DMPC bilayer. 1D ^{19}F cross sections at the lipid CH_2 and water ^{1}H chemical shifts are shown on the right of each 2D spectrum. The two DMPC samples show much higher lipid cross peaks compared to the VMS^{cluster} samples. The VMS^{cluster} 2D spectra (a, c) were measured at 275 K whereas the DMPC 2D spectra (b, d) were measured at 290 K. 1D ^{1}H spectra of the two types of membranes at these temperatures show similar ^{1}H linewidths for the lipid chain CH_2 peak, indicating that the lipid chain dynamics is similar at these temperatures.

residue of the peptide relative to the bilayer center. Figure 6 shows the results of the simulations for a single gp41 trimer. At 303 K, the center of MPER lies at 19 and 12 Å from the bilayer center in the VMS^{cluster} and DMPC membranes, respectively (Figure 6(a, c)). The VMS^{cluster} membrane is only 5.1 Å thicker than the DMPC bilayer: the distance from the membrane center to the average phosphorus position in each leaflet is 22.8 Å for the VMS^{cluster} membrane and 17.7 Å for DMPC at 303 K. Thus, these results indicate that the MPER is less embedded in the VMS^{cluster} membrane than in the DMPC bilayer, consistent with the solid-state NMR data. In addition, the MPER orientation is more parallel to the membrane surface in the VMS^{cluster} membrane: the average angle θ between the helix axis and the bilayer normal is 70° in the VMS^{cluster} membrane but decreases to 45° in the DMPC membrane (Figure 6(d–f)). This orientational change is consistent with the depth difference of the peptide between the two membranes.

To test whether these differences in MPER orientation and depth of insertion are due to cholesterol, we carried out simulations in a modified, cholesterol-free, VMS^{cluster} membrane. As shown in Figure 6(b and d), excluding cholesterol from the membrane led to a pronounced decrease of the average Z positions of MPER residues as well as a reduction of the θ angle compared to the results in the cholesterol-containing VMS^{cluster} membrane. As illustrated by the snapshots in Figure 6(e), binding of cholesterol to the helix-turn-helix region of the peptide tends to orient the MPER parallel to the membrane surface, and reduces its insertion into the hydrophobic region of the bilayer. These trends are qualitatively maintained in the 280 K simulations (Figures S4 and S5), although the orientational difference is smaller in the low-

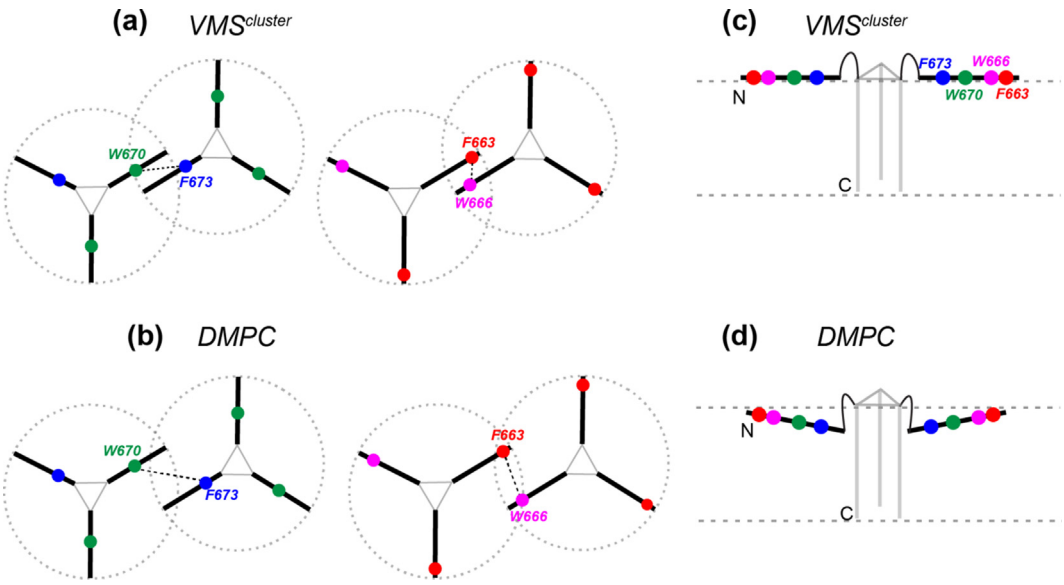

Figure 5. Models of gp41 MPER-TMD trimer clustering (a, b) and MPER depth of insertion (c, d) in lipid membranes. (a, c) VMS^{cluster} membrane. (b, d) DMPC membrane. Two gp41 trimers cluster to cause partial interdigitation of the MPER. The trimers approach each other more closely in the VMS^{cluster} membrane than in the DMPC membrane. The MPER helices are more deeply inserted in the DMPC bilayer than in the VMS^{cluster} membrane.

temperature simulations, in part because the DMPC membrane is in the gel phase at 280 K (Figure S6). These simulations thus support the physiological relevance of the solid-state NMR measurements at low temperatures.

All-atom molecular dynamics simulations reveal that multiple MPER-TMD trimers indeed cluster in the membrane; moreover, this self-association is facilitated by cholesterol. To characterize the separation between two trimers, we monitored two quantities: the distribution of pairwise distances between all Cα atoms in adjacent MPERs, and the distribution of distances between W680 Cα distances in adjacent MPERs (Figure 7(a)). The latter is particularly robust against MPER lateral fluctuations, since W680 is near the turn between the MPER and the TMD. Both these distance parameters are more stable than the inter-trimer W670-F673 and W666-F663 distances measured in the 2D ^{19}F-^{19}F correlation NMR experiments, which are sensitive to fluctuations of the MPER helix at the sluggish membrane-water interface.

Figure 7(b) shows that the Cα-Cα distance distribution is broader in the DMPC membrane than in the VMS^{cluster} membrane, suggesting that two MPERs from two trimers are more tightly associated in the VMS^{cluster} membrane. The distance distributions between adjacent W680 Cα atoms (Figure 7(c)) show an even clearer trend: the average separation is 3.0 nm in the VMS^{cluster} membrane, which increases to 3.9 nm in the DMPC membrane and 4.1 nm in the cholesterol-free VMS^{cluster} membrane. Therefore, the MPER-TMD trimers cluster more tightly in cholesterol-containing membranes than in cholesterol-free membranes. Moreover, when the clustered dimer of trimers in the VMS^{cluster} membrane is embedded in cholesterol-free membranes, the distance between the two trimers quickly increased in independent simulations (Figure S7). As the snapshot in Figure 7(d, f) illustrates, cholesterol molecules occasionally interact simultaneously with the MPER motifs from two trimers. CG simulations (Figure S2) confirm this favorable interaction between gp41 and cholesterol, showing an enhancement of the cholesterol concentration near gp41 compared to the bulk.

Discussion

These solid-state NMR data (Figures 3 and 4) and molecular dynamics simulations provide direct experimental evidence for the clustering of gp41 MPER-TMD trimers in lipid bilayers. The 2D ^{19}F-^{19}F spin diffusion NMR spectra, which are sensitive to inter-fluorine distances up to ~2 nm,[50] give residue-specific information about trimer-trimer association on the nanometer scale. The observation of ^{19}F-^{19}F correlation peaks between W670 and F673 at the center of two different MPER helices, and between F663 and W666 near the N-terminus of two MPER helices, indicates that multiple trimers cluster to intercalate their MPER helices (Figure 5). Importantly, these ^{19}F-^{19}F correlation peaks are observed in the cholesterol-containing VMS^{cluster} membrane but are mostly suppressed in the DMPC membrane at the same P/L molar

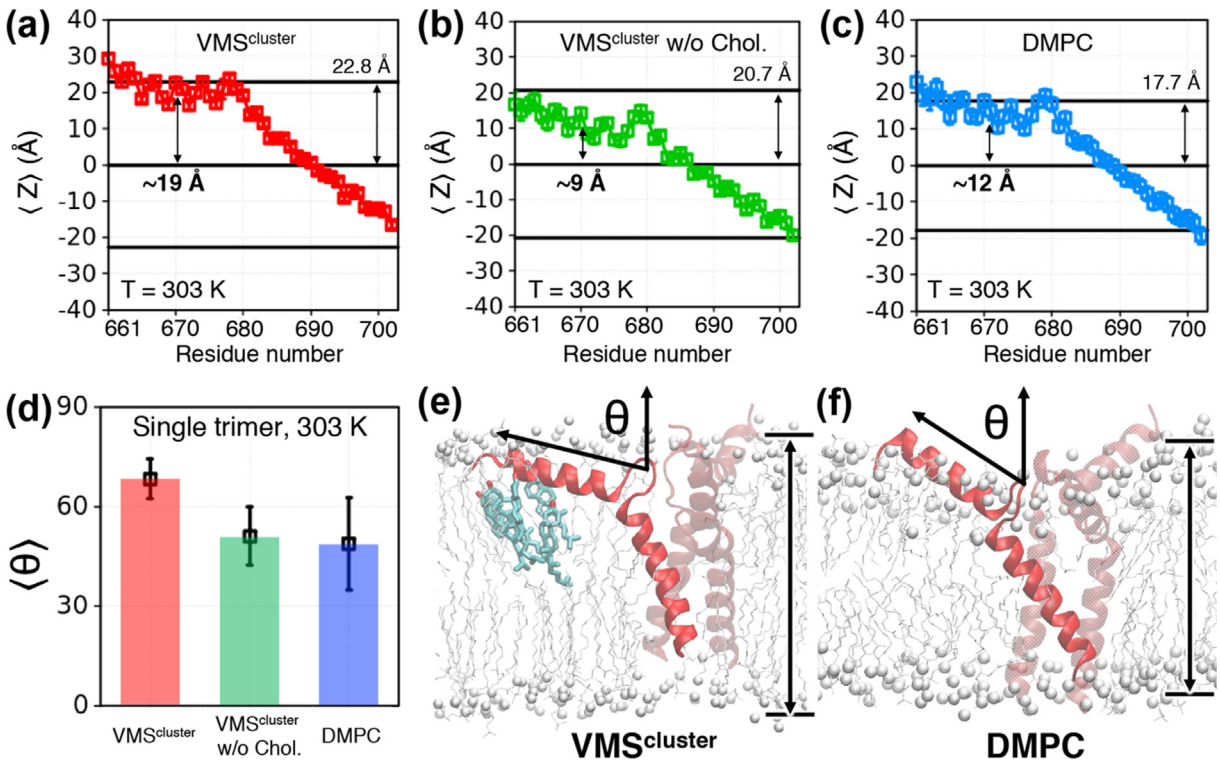

Figure 6. All-atom simulations at 303 K of a single gp41 MPER-TMD trimer indicate that the MPER orientation is perturbed by cholesterol. Simulations at 280 K give qualitatively similar results and are summarized in Figure S4. (a–c) Z coordinates of all atoms in each residue, averaged over three peptide chains along independent MD trajectories. A single gp41 trimer is embedded in the (a) VMS^{cluster} membrane, (b) cholesterol-free VMS^{cluster} membrane, and (c) DMPC membrane. Statistical errors of the Z coordinates are similar in magnitude as the size of each box symbol. The membrane center is taken to be Z = 0, and the membrane thickness, defined by the location of P atoms in the two leaflets, is indicated by horizontal solid lines. (d) Average angle θ between the MPER helix and the membrane normal, which is defined as the Z axis of the simulation box. The Cα atoms of the first and last 4 residues (L661-D664 and A677-W680) of MPER are used to define the helical axis. (e, f) Snapshots from VMS^{cluster} and DMPC simulations illustrate the different locations of the MPER and the locations of nearby (within 2.5 Å of MPER) cholesterol molecules in the VMS^{cluster} membrane. Phosphate atoms are shown as white spheres and lipid tails are shown as thin lines.

ratios (Figure 3). This difference indicates that these intermolecular cross peaks do not result from the same trimer nor reflect the average separation of homogeneously distributed trimers in the lipid membrane. Rather, they result from the close approach of multiple MPER-TMD trimers in the presence of cholesterol. This association involves inter-fluorine distances of less than 2 nm, which is shorter than the average separation at the P/L ratio of 1:30 used here.

The clustering of the MPER-TMD trimers in the cholesterol-containing membrane correlates with the more surface-exposed location of the MPER in the VMS^{cluster} membrane compared to the DMPC membrane. 2D ^{1}H-^{19}F HETCOR spectra show that the MPER residues have much weaker cross peaks with lipid acyl chains in the VMS^{cluster} membrane than in the DMPC membrane (Figures 4 and 5(c, d)). Atomistic simulations confirm that the MPER helix is more parallel to the membrane surface in the VMS^{cluster} bilayer but is more tilted and buried in the DMPC bilayer (Figure 6). The more in-plane orientation extends the MPER reach, thus promoting trimer-trimer interactions. The fact that cholesterol lifts and extends the MPER to the membrane surface is in excellent agreement with the location of cholesterol under the canopy of the MPER helix, as found in the recent solid-state NMR and molecular dynamic study.[24] The simulations in that study identified two hotspots of interaction with cholesterol, ^{673}-FNITN^{677} in the MPER and ^{684}LFIMI^{688} in the TMD. These two hotspots flank the turn between the MPER and TMD and sequester cholesterol in the L-shaped fold, in analogy with the mode of interaction between the influenza M2 protein and cholesterol.[56,57]

The limited sensitivity of ^{19}F exchange NMR experiments for measuring nanometer ^{19}F-^{19}F contacts prohibit a more exhaustive study of the lipid dependence and peptide-concentration dependence of gp41 trimer clustering. Instead, molecular dynamics simulations fill this gap. All-atom simulations show that the MPER-TMD

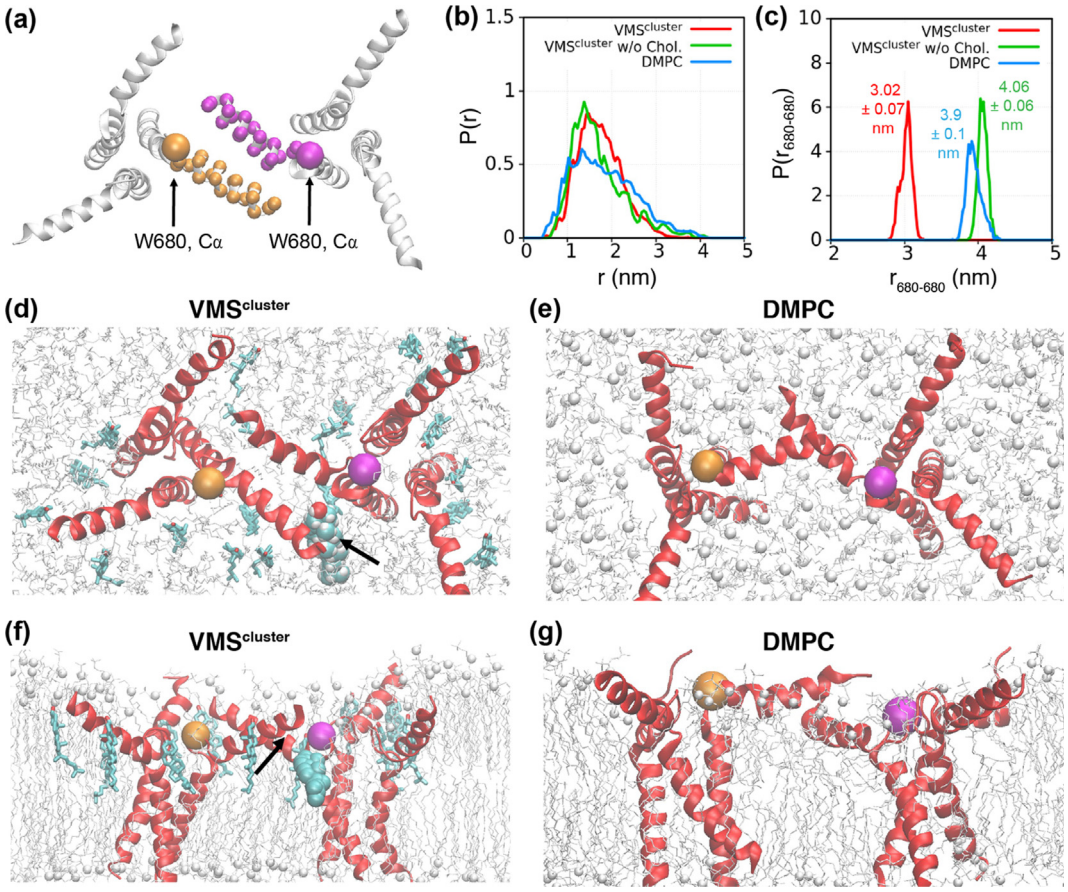

Figure 7. Association of two MPER-TMD trimers in all-atom simulations at 303 K. (a) Snapshot illustrating the displacement of two gp41 trimers from the simulations. Small spheres indicate the Cα atoms in adjacent MPERs whereas big spheres represent the Cα atoms of W680 near the C-terminal end of the MPER. (b) Probability distribution of pairwise distances between all Cα atoms in adjacent MPERs of two gp41 trimers, as shown in panel (a). (c) Probability distribution of W680-W680 Cα-Cα distances between two gp41 trimers, as shown in panel (a). The results at 280 K are qualitatively similar and are shown in Figure S4. (d, e) Top view of snapshots for the dimer of trimers in the VMS^{cluster} and DMPC membranes, respectively. Cholesterols within 5 Å of any atoms of MPER are shown, and in some cases, cholesterol is observed to interact with both MPERs. (f, g) Sideview of the snapshots. These snapshots indicate that close MPER contacts form only through inter-trimer interactions, supporting the result of the solid-state NMR analysis (Figure 5).

trimers cluster at an even lower P/L molar ratio of 1:70 (Figure 7(d), Table 3), supporting the notion that this trimer clustering is relevant under biological conditions. Removal of cholesterol from the VMS^{cluster} membrane increased the average inter-trimer W680-W680 distances to 4.1 nm, similar to the average distance of 3.9 nm in DMPC bilayers (Figure 7(c)). In the VMS^{cluster} membrane, cholesterol molecules are observed to interact occasionally with adjacent MPERs of two trimers. Such bridging configurations may combine with cholesterol's indirect modulation of the orientation of the MPER helix to facilitate trimer clustering. A recent coarse-grained simulation of full-length gp41 in a virus-mimetic membrane showed that at least three gp41 trimers are required to cause membrane fusion.[58] Lipid stalk formation was observed when multiple trimers approached each other within ~3.5 nm, measured from the center of mass of each trimer. In our current all-atom simulations, the distance between the centers of the TM helical bundle is 3.8–4.3 nm, in good agreement with the results of the previous coarse-grained simulations.

Our current finding that membrane cholesterol promotes the clustering of MPER-TMD trimers is consistent with previous fluorescence spectroscopy data that cholesterol enhanced the fusion activity of the MPER and promoted its self-association.[23] It is also consistent with a large amount of biochemical data that indicate that gp41 localizes to the edge of the cholesterol-rich, liquid-ordered region of the membrane.[24] The VMS^{cluster} membrane in our NMR experiments and simulations contains 30 mol% cholesterol and 20 mol% SM. Although the phase diagram of this exact lipid

mixture has not been characterized, based on the ternary phase diagram of POPC/PSM/cholesterol,[59] the $VMS^{cluster}$ membrane likely contains both L_d and L_o phases.[60–62] Explicitly probing the preferential localization of gp41 to different lipid domains would require much larger systems that are computationally expensive at the atomistic level. As an alternative approach,[63] our coarse-grained simulations found that the cholesterol concentrations near gp41 are substantially elevated compared to the bulk (Figure S2), confirming that gp41 preferentially interacts with cholesterol. Combining these solid-state NMR data and simulations, we propose that complexation between the MPER and cholesterol induces lateral segregation of gp41 to cholesterol-rich regions of the lipid membrane and anchors the MPER at the membrane surface for self-association. In addition to cholesterol, the amino acid sequence of the MPER may also play a role in clustering. For example, a recent NMR study found that trimerization of the MPER peptide in solution requires hydrophobic interactions involving two N-terminal Leu residues.[64] Our simulations indicate that I665, D664, S668, N671 and W672 are predominantly involved in trimer-trimer contacts (Figure S8), suggesting that both hydrophobic and polar interactions contribute to MPER clustering. Therefore, gp41 clustering may be promoted by the concerted action of the cholesterol-rich membrane and the MPER amino acid sequence.

How does clustering of MPER-TMD trimers mediate membrane fusion? We propose that multiple gp41 trimers, brought together by the cholesterol dimers and tetramers discovered recently,[65] amplify positive membrane curvature prior to the formation of the hemifusion intermediate. We speculate that this positive membrane curvature is caused by the shallow insertion of the MPER helix and the large radial footprint of each MPER-TMD trimer.[66,67] This positive membrane curvature favors the close juxtaposition of the viral membrane and host-cell membrane. Interdigitation of the MPER helices between the clustered trimers may enable the coordinated bending of a larger lipid surface area compared to an end-to-end arrangement of the MPER helices. Clustering of MPER-TMD may also further enrich cholesterol, thus causing increased lipid asymmetry. Thus, clustering of gp41 MPER-TMD may promote virus-cell membranes fusion by generating both membrane curvature and lipid asymmetry.

CRediT authorship contribution statement

Nhi Tran: Data curation, Formal analysis, Validation, Writing: original draft. **Younghoon Oh:** Data curation, Formal analysis, Validation, Writing: original draft. **Madeleine Sutherland:** Data curation, Validation. **Qiang Cui:** Conceptulization, Funding acquisition, Supervision, Validation, Review and editing. **Mei Hong:** Conceptulization, Funding acquisition, Supervision,Validation, Review and editing.

Acknowledgements

This work is supported by NIH grant GM066976 to M.H. The computational work and Y.O. are supported in part by the NSF grant CHE-1829555 to Q.C. Computational resources from the Extreme Science and Engineering Discovery Environment (XSEDE), which is supported by NSF grant number OCI-1053575, are greatly appreciated. Part of the computational work was performed on the Shared Computing Cluster which is administered by Boston University's Research Computing Services (URL: www.bu.edu/tech/support/research/).

Declaration of interests

The authors declare that they have no known competing financial interests or personal relationships that could have appeared to influence the work reported in this paper.

Appendix A. Supplementary material

Supplementary data to this article can be found online at https://doi.org/10.1016/j.jmb.2021.167345.

Received 2 October 2021;
Accepted 31 October 2021;
Available online 8 November 2021

Keywords:
^{19}F solid-state NMR;
MPER;
membrane protein clustering;
virus-cell fusion

References

1. Simons, K., Toomre, D., (2000). Lipid rafts and signal transduction. *Nature Rev. Mol. Cell Biol.* **1**, 31–39.
2. Sezgin, E., Levental, I., Mayor, S., Eggeling, C., (2017). The mystery of membrane organization: composition, regulation and roles of lipid rafts. *Nature Rev. Mol. Cell Biol.* **18**, 361–374.
3. Head, B.P., Patel, H.H., Insel, P.A., (2014). Interaction of membrane/lipid rafts with the cytoskeleton: Impact on signaling and function: Membrane/lipid rafts, mediators of cytoskeletal arrangement and cell signaling. *Biochim. Biophys. Acta* **1838**, 532–545.
4. Lingwood, D., Simons, K., (2010). Lipid Rafts As a Membrane-Organizing Principle. *Science* **327**, 46.

5. Hua, Y., Scheller, R.H., (2001). Three SNARE complexes cooperate to mediate membrane fusion. *Proc. Natl. Acad. Sci. U.S.A.* **98**, 8065.
6. Milovanovic, D., Honigmann, A., Koike, S., Göttfert, F., Pähler, G., Junius, M., et al., (2015). Hydrophobic mismatch sorts SNARE proteins into distinct membrane domains. *Nature Commun.* **6**, 5984.
7. van den Bogaart, G., Meyenberg, K., Risselada, H.J., Amin, H., Willig, K.I., Hubrich, B.E., et al., (2011). Membrane protein sequestering by ionic protein–lipid interactions. *Nature.* **479**, 552–555.
8. Ono, A., Freed, E.O., (2005). Role of Lipid Rafts in Virus Replication. *Adv. Virus Res.*, 311–358.
9. Campbell, S.M., Crowe, S.M., Mak, J., (2001). Lipid rafts and HIV-1: from viral entry to assembly of progeny virions. *J. Clin. Virol.* **22**, 217–227.
10. Waheed, A.A., Freed, E.O., (2009). Lipids and membrane microdomains in HIV-1 replication. *Virus Res.* **143**, 162–176.
11. Cheng, R.H., Kuhn, R.J., Olson, N.H., Rossmann, M.G., Choi, H.K., Smith, T.J., et al., (1995). Nucleocapsid and glycoprotein organization in an enveloped virus. *Cell* **80**, 621–630.
12. Harris, A., Cardone, G., Winkler, D.C., Heymann, J.B., Brecher, M., White, J.M., et al., (2006). Influenza virus pleiomorphy characterized by cryoelectron tomography. *Proc. Natl. Acad. Sci. U.S.A.* **103**, 19123.
13. Sougrat, R., Bartesaghi, A., Lifson, J.D., Bennett, A.E., Bess, J.W., Zabransky, D.J., et al., (2007). Electron Tomography of the Contact between T Cells and SIV/HIV-1: Implications for Viral Entry. *PLoS Pathog.* **3**, e63.
14. Chojnacki, J., Staudt, T., Glass, B., Bingen, P., Engelhardt, J., Anders, M., et al., (2012). Maturation-Dependent HIV-1 Surface Protein Redistribution Revealed by Fluorescence Nanoscopy. *Science* **338**, 524.
15. Chojnacki, J., Waithe, D., Carravilla, P., Huarte, N., Galiani, S., Enderlein, J., et al., (2017). Envelope glycoprotein mobility on HIV-1 particles depends on the virus maturation state. *Nature Commun.* **8**, 545.
16. Nieto-Garai, J.A., Arboleya, A., Otaegi, S., Chojnacki, J., Casas, J., Fabriàs, G., et al., (2021). Cholesterol in the Viral Membrane is a Molecular Switch Governing HIV-1 Env Clustering. *Adv. Sci.* **8**, 2003468.
17. Wyma, D.J., Jiang, J., Shi, J., Zhou, J., Lineberger, J.E., Miller, M.D., et al., (2004). Coupling of Human Immunodeficiency Virus Type 1 Fusion to Virion Maturation: a Novel Role of the gp41 Cytoplasmic Tail. *J. Virol.* **78**, 3429.
18. Murakami, T., Ablan, S., Freed, E.O., Tanaka, Y., (2004). Regulation of Human Immunodeficiency Virus Type 1 Env-Mediated Membrane Fusion by Viral Protease Activity. *J. Virol.* **78**, 1026.
19. Kwon, B., Lee, M., Waring, A.J., Hong, M., (2018). Oligomeric Structure and Three-Dimensional Fold of the HIV gp41 Membrane-Proximal External Region and Transmembrane Domain in Phospholipid Bilayers. *J. Am. Chem. Soc.* **140**, 8246–8259.
20. Sun, Z.Y., Oh, K.J., Kim, M., Yu, J., Brusic, V., Song, L., et al., (2008). HIV-1 broadly neutralizing antibody extracts its epitope from a kinked gp41 ectodomain region on the viral membrane. *Immunity* **28**, 52–63.
21. Suárez, T., Gallaher, W.R., Agirre, A., Goñi, F.M., Nieva, J. L., (2000). Membrane Interface-Interacting Sequences within the Ectodomain of the Human Immunodeficiency Virus Type 1 Envelope Glycoprotein: Putative Role during Viral Fusion. *J. Virol.* **74**, 8038.
22. Epand, R.M., Sayer, B.G., Epand, R.F., (2003). Peptide-induced formation of cholesterol-rich domains. *Biochemistry* **42**, 14677–14689.
23. Saez-Cirion, A., Nir, S., Lorizate, M., Agirre, A., Cruz, A., Perez-Gil, J., et al., (2002). Sphingomyelin and cholesterol promote HIV-1 gp41 pretransmembrane sequence surface aggregation and membrane restructuring. *J. Biol. Chem.* **277**, 21776–21785.
24. Kwon, B., Mandal, T., Elkins, M.R., Oh, Y., Cui, Q., Hong, M., (2020). Cholesterol Interaction with the Trimeric HIV Fusion Protein gp41 in Lipid Bilayers Investigated by Solid-State NMR Spectroscopy and Molecular Dynamics Simulations. *J. Mol. Biol.* **432**, 4705–4721.
25. Campbell, S.M., Crowe, S.M., Mak, J., (2002). Virion-associated cholesterol is critical for the maintenance of HIV-1 structure and infectivity. *AIDS* **16**, 2253–2261.
26. Liao, Z.H., Cimakasky, L.M., Hampton, R., Nguyen, D.H., Hildreth, J.E.K., (2001). Lipid rafts and HIV pathogenesis: Host membrane cholesterol is required for infection by HIV type 1. *AIDS Res. Hum. Retrovir.* **17**, 1009–1019.
27. Liao, Z.H., Graham, D.R., Hildreth, J.E.K., (2003). Lipid rafts and HIV pathogenesis: Virion-associated cholesterol is required for fusion and infection of susceptible cells. *AIDS Res. Hum. Retrovir.* **19**, 675–687.
28. Zheng, Y.-H., Plemenitas, A., Fielding, C.J., Peterlin, B.M., (2003). Nef increases the synthesis of and transports cholesterol to lipid rafts and HIV-1 progeny virions. *Proc. Natl. Acad. Sci. U.S.A.* **100**, 8460.
29. Mijalis, A.J., Thomas 3rd, D.A., Simon, M.D., Adamo, A., Beaumont, R., Jensen, K.F., et al., (2017). A fully automated flow-based approach for accelerated peptide synthesis. *Nature Chem. Biol.* **13**, 464–466.
30. Brugger, B., Glass, B., Haberkant, P., Leibrecht, I., Wieland, F.T., Krausslich, H.G., (2006). The HIV lipidome: A raft with an unusual composition. *Proc. Natl. Acad. Sci. U.S.A.* **103**, 2641–2646.
31. Aloia, R.C., Tian, H., Jensen, F.C., (1993). Lipid composition and fluidity of the human immunodeficiency virus envelope and host cell plasma membranes. *Proc. Natl. Acad. Sci. U.S.A.* **90**, 5181.
32. Bennett, A.E., Rienstra, C.M., Auger, M., Lakshmi, K.V., Griffin, R.G., (1995). Heteronuclear decoupling in rotating solids. *J. Chem. Phys.* **103**, 6951–6958.
33. Hou, G., Yan, S., Trebosc, J., Amoureux, J.P., Polenova, T., (2013). Broadband homonuclear correlation spectroscopy driven by combined R2(n)(v) sequences under fast magic angle spinning for NMR structural analysis of organic and biological solids. *J. Magn. Reson.* **232**, 18–30.
34. Huster, D., Yao, X.L., Hong, M., (2002). Membrane Protein Topology Probed by 1H Spin Diffusion from Lipids Using Solid-State NMR Spectroscopy. *J. Am. Chem. Soc.* **124**, 874–883.
35. Hong, M., Schmidt-Rohr, K., (2013). Magic-angle-spinning NMR techniques for measuring long-range distances in biological macromolecules. *Acc. Chem. Res.* **46**, 2154–2163.
36. Doherty, T., Hong, M., (2009). 2D (1)H-(31)P solid-state NMR studies of the dependence of inter-bilayer water dynamics on lipid headgroup structure and membrane peptides. *J. Magn. Reson.* **196**, 39–47.

37. Lesage, A., Bockmann, A., (2003). Water-protein interactions in microcrystalline Crh measured by H-1-C-13 solid-state NMR spectroscopy. *J. Am. Chem. Soc.* **125**, 13336–13337.
38. Jo, S., Kim, T., Iyer, V.G., Im, W., (2008). CHARMM-GUI: a web-based graphical user interface for CHARMM. *J. Comput. Chem.* **29**, 1859–1865.
39. Jo, S., Lim, J.B., Klauda, J.B., Im, W., (2009). CHARMM-GUI Membrane Builder for mixed bilayers and its application to yeast membranes. *Biophys. J.* **97**, 50–58.
40. Huang, J., MacKerell Jr., A.D., (2013). CHARMM36 all-atom additive protein force field: Validation based on comparison to NMR data. *J. Comput. Chem.* **34**, 2135–2145.
41. Klauda, J.B., Venable, R.M., Freites, J.A., O'Connor, J.W., Tobias, D.J., Mondragon-Ramirez, C., et al., (2010). Update of the CHARMM all-atom additive force field for lipids: validation on six lipid types. *J. Phys. Chem. B* **114**, 7830–7843.
42. Jorgensen, W.L., Chandrasekhar, J., Madura, J.D., Impey, R.W., Klein, M.L., (1983). Comparison of simple potential functions for simulating liquid water. *J. Chem. Phys.* **79**, 926–935.
43. Ohkubo, Y.Z., Pogorelov, T.V., Arcario, M.J., Christensen, G.A., Tajkhorshid, E., (2012). Accelerating membrane insertion of peripheral proteins with a novel membrane mimetic model. *Biophys. J.* **102**, 2130–2139.
44. Qi, Y., Cheng, X., Lee, J., Vermaas, J.V., Pogorelov, T.V., Tajkhorshid, E., et al., (2015). CHARMM-GUI HMMM Builder for Membrane Simulations with the Highly Mobile Membrane-Mimetic Model. *Biophys. J.* **109**, 2012–2022.
45. Parrinello, M., Rahman, A., (1981). Polymorphic transitions in single crystals: A new molecular dynamics method. *J. Appl. Phys.* **52**, 7182–7190.
46. Nose, S., (1984). A unified formulation of the constant temperature molecular dynamics methods. *J. Chem. Phys.* **81**, 511–519.
47. Hoover, W.G., (1985). Canonical dynamics: Equilibrium phase-space distributions. *Phys. Rev. A* **31**, 1695–1697.
48. Hess, B., Bekker, H., Berendsen, H.J.C., Fraaije, J.G.E.M., (1997). LINCS: a linear constraint solver for molecular simulations. *J. Comput. Chem.* **18**, 1463–1472.
49. Spoel, D.V.D., Lindahl, E., Hess, B., Groenhof, G., Mark, A. E., Berendsen, H.J.C., (2005). GROMACS: Fast, flexible, and free. *J. Comp. Chem.* **2005**, 1701–1718.
50. Roos, M., Wang, T., Shcherbakov, A.A., Hong, M., (2018). Fast Magic-Angle-Spinning (19)F Spin Exchange NMR for Determining Nanometer (19)F-(19)F Distances in Proteins and Pharmaceutical Compounds. *J. Phys. Chem. B* **122**, 2900–2911.
51. Wang, M., Lu, M., Fritz, M., Quinn, C., Byeon, I.J., Byeon, C.H., et al., (2018). Fast Magic Angle Spinning ^{19}F NMR of HIV-1 Capsid Protein Assemblies. *Angew. Chem. Int. Ed. Engl.* **57**, 16375–16379.
52. Fu, Q., Shaik, M.M., Cai, Y., Ghantous, F., Piai, A., Peng, H., et al., (2018). Structure of the membrane proximal external region of HIV-1 envelope glycoprotein. *Proc. Natl. Acad. Sci. U.S.A.* **115**, E8892.
53. Chiliveri, S.C., Louis, J.M., Ghirlando, R., Baber, J.L., Bax, A., (2018). Tilted, Uninterrupted, Monomeric HIV-1 gp41 Transmembrane Helix from Residual Dipolar Couplings. *J. Am. Chem. Soc.* **140**, 34–37.
54. Aisenbrey, C., Rifi, O., Bechinger, B., (2020). Structure, membrane topology and influence of cholesterol of the membrane proximal region: transmembrane helical anchor sequence of gp41 from HIV. *Sci. Rep.* **10**, 22278.
55. Sirota, E.B., Smith, G.S., Safinya, C.R., Plano, R.J., Clark, N.A., (1988). X-ray Scattering Studies of Aligned, Stacked Surfactant Membranes. *Science* **242**, 1406–1409.
56. Elkins, M.R., Williams, J.K., Gelenter, M.D., Dai, P., Kwon, B., Sergeyev, I.V., et al., (2017). Cholesterol-binding site of the influenza M2 protein in lipid bilayers from solid-state NMR. *Proc. Natl. Acad. Sci. U.S.A.* **114**, 12946–12951.
57. Elkins, M.R., Sergeyev, I.V., Hong, M., (2018). Determining Cholesterol Binding to Membrane Proteins by Cholesterol (13)C Labeling in Yeast and Dynamic Nuclear Polarization NMR. *J. Am. Chem. Soc.* **140**, 15437–15449.
58. Gorai, B., Sahoo, A.K., Srivastava, A., Dixit, N.M., Maiti, P. K., (2021). Concerted Interactions between Multiple gp41 Trimers and the Target Cell Lipidome May Be Required for HIV-1 Entry. *J. Chem. Inf. Model.* **61**, 444–454.
59. de Almeida, R.F.M., Fedorov, A., Prieto, M., (2003). Sphingomyelin/Phosphatidylcholine/Cholesterol Phase Diagram: Boundaries and Composition of Lipid Rafts. *Biophys. J.* **85**, 2406–2416.
60. Veatch, S.L., Keller, S.L., (2005). Seeing spots: Complex phase behavior in simple membranes. *Biochim. Biophys. Acta* **1746**, 172–185.
61. Feigenson, G.W., (2009). Phase diagrams and lipid domains in multicomponent lipid bilayer mixtures. *Biochim. Biophys. Acta – Biomem.* **1788**, 47–52.
62. Meyer, F.-J.-M., Benjamini, A., Rodgers, J.M., Misteli, Y., Smit, B., (2010). Molecular Simulation of the DMPC-Cholesterol Phase Diagram. *J. Phys. Chem. B* **114**, 10451–10461.
63. Corradi, V., Mendez-Villuendaas, E., Ingolfsson, H.I., Gu, R., Siuda, I., Melo, M.N., et al., (2018). Lipid−Protein Interactions Are Unique Fingerprints for Membrane Proteins. *ACS Central Sci.* **4**, 709–717.
64. Chiliveri, S.C., Louis, J.M., Bax, A., (2021). Concentration-Dependent Structural Transition of the HIV-1 gp41 MPER Peptide into α-Helical Trimers. *Angew. Chem. Int. Ed.* **60**, 166–170.
65. Elkins, M.R., Bandara, A., Pantelopulos, G.A., Straub, J.E., Hong, M., (2021). Direct Observation of Cholesterol Dimers and Tetramers in Lipid Bilayers. *J. Phys. Chem. B* **125**, 1825–1837.
66. Campelo, F., McMahon, H.T., Kozlov, M.M., (2008). The Hydrophobic Insertion Mechanism of Membrane Curvature Generation by Proteins. *Biophys. J.* **95**, 2325–2339.
67. Mandal, T., Spagnolie, S.E., Audhya, A., Cui, Q., (2021). Protein Induced Membrane Curvature in Coarse-Grained Simulations: Binding Interface, Insertion Depth and Lipid Spontaneous Curvature. *Biophys. J.* **120**, 3211–3221.

Supporting Information

Cholesterol-Mediated Clustering of the HIV Fusion Protein gp41 in Lipid Bilayers

Nhi Tran [1], Younghoon Oh [2], Madeleine Sutherland [1], Qiang Cui [2,3,4] *, and Mei Hong [1]*

[1] Department of Chemistry, Massachusetts Institute of Technology, 170 Albany Street, Cambridge, MA 02139

[2] Department of Chemistry, [3] Department of Physics and [4] Department of Biomedical Engineering, Boston University, 590 Commonwealth Avenue, Boston, MA 02215

Coarse-grained molecular dynamics simulations

Coarse-grained (CG) molecular dynamics simulations for gp41 in various membranes were carried out using the MARTINI v2.2 model [1, 2] to complement the atomistic simulations discussed in the main text. First, CG simulations were used to efficiently explore various dimerization orientations. Then the most stable one was selected for further atomistic simulations. Second, CG simulations with larger system dimensions were used to better sample lipid and cholesterol distributions near gp41 relative to the bulk.

To explore different dimerization orientations, nine gp41 trimers were evenly distributed [3] in the lipid membrane with a lateral dimension of 20 nm × 20 nm, and the system was simulated for 25 μs of production MD runs to probe different association patterns. As shown in **Fig. S1,** the gp41 trimers were observed to quickly aggregate into a large cluster, which feature three representative types of relative orientations during the production runs. We then selected the orientation that features the most extensive gp41-gp41 contacts for further characterization at the atomistic level. We are aware of the fact that MARTINI v2.2 is known for overestimating the association of transmembrane proteins [4, 5]. The goal of this study, however, is not to determine the size distribution of gp41 clusters; rather, we use the CG simulations to efficiently explore possible dimer configurations, which are then subject to more accurate atomistic simulations. The comparison of results using other MARTINI models, including both MARTINI 3[6] and a revised MARTINI v2.2 model with reduced protein association [7], will be reported elsewhere.

To probe local cholesterol and lipid distributions, we introduced either a single gp41 trimer into a membrane with the lateral dimension 10 nm × 10 nm, or a dimer of gp41 trimers into a membrane of 12 nm ×12 nm. Weak harmonic restraints (with a force constant of 1 kJ mol^{-1} nm^{-2}) were applied to the protein backbone beads to efficiently sample the local condensation patterns of membrane components during 25 μs of production MD simulations. The restraint is sufficiently weak to allow local motion of the protein without affecting the binding-unbinding equilibrium of lipids and cholesterol to protein.[8, 9]

In these CG simulations, the structural model of the gp41 trimer is constructed based on the previous solid-state NMR study (PDB: 6DLN) [10]. The lipid membranes are composed of

POPC, POPE, PSM, and cholesterol with a molar ratio 10:10:10:13, which are similar but not identical to the atomistic simulations reported in the main text; the impact on the key trends of interest is expected to be minimal. Initial configurations were built using CHARMM-GUI [11, 12], with a water layer of 22.5 Å on each side of the bilayer and a NaCl concentration of 150 mM. All simulations were conducted using the GROMACS-2018.3 molecular dynamics simulation software [13]. Each CG system was first energy minimized, followed by 1 μs of equilibration before production runs. Berendsen thermostat and barostat [14] were employed for equilibration, while for the production runs, velocity rescale thermostat [15] and Parrinello-Rahman barostat [16] were used instead.

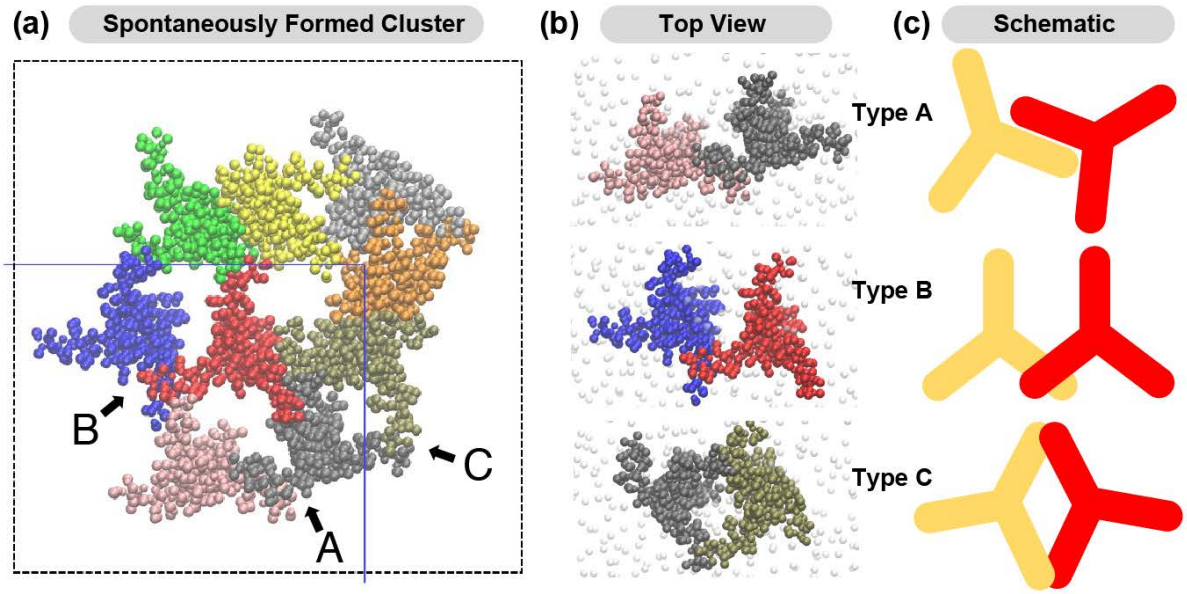

Fig. S1. Results of coarse-grained simulations of gp41 trimers in a multi-component membrane. (**a**) A snapshot illustrating the spontaneous clustering of multiple gp41 trimers, which were evenly distributed at the beginning of the simulation with an approximate separation of 5-6 nm. (**b**) Representative dimer of trimer configurations sampled in the 25 μs simulations. (**c**) All dimers of trimers can be schematically classified into the three categories. Class A features the most extensive trimer-trimer interactions and therefore was further analyzed with atomistic simulations in the main text.

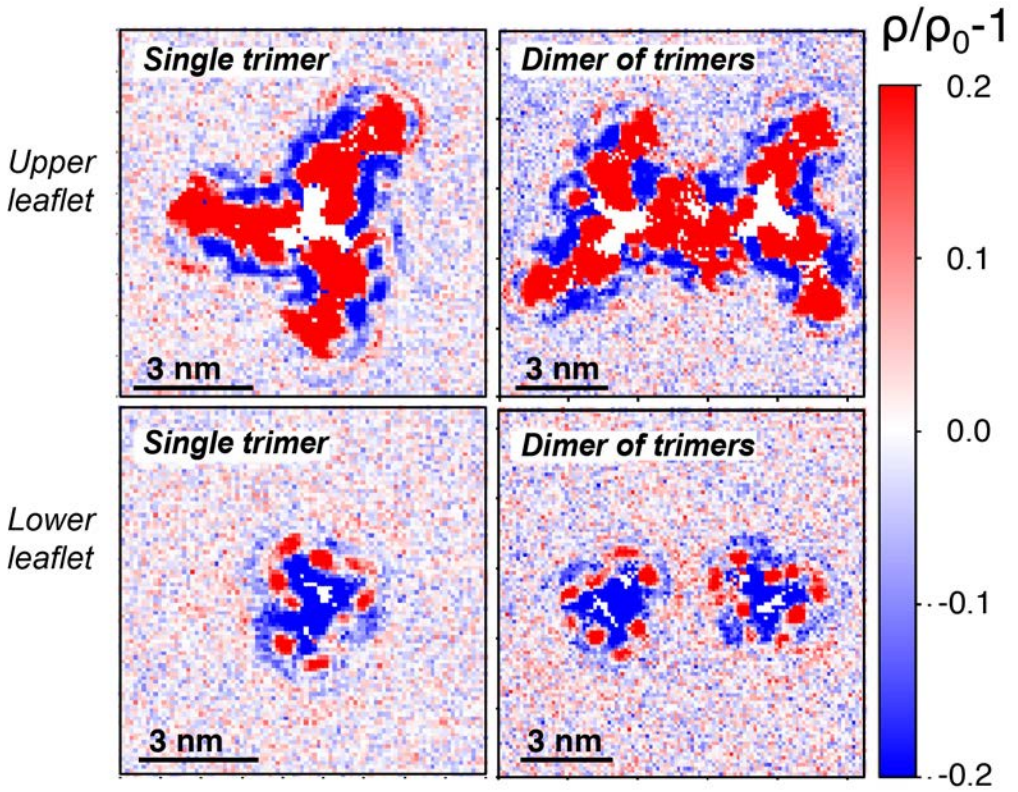

Fig. S2. Coarse-grained simulations showing differences in the cholesterol density (ρ/ρ_0-1) near a gp41 trimer (left) and a dimer of gp41 trimers (right) relative to the bulk. ρ_0 is the bulk cholesterol density. Red indicates enhancement of the cholesterol concentration relative to the bulk value whereas blue indicates reduction of cholesterol concentration. Top and bottom rows show the results for the upper and lower leaflets of the membrane, respectively. The results highlight the favorable interaction between cholesterol and gp41, especially the MPER motifs, which cause substantial increase of the local cholesterol concentration in the upper leaflet of the membrane where the MPER resides.

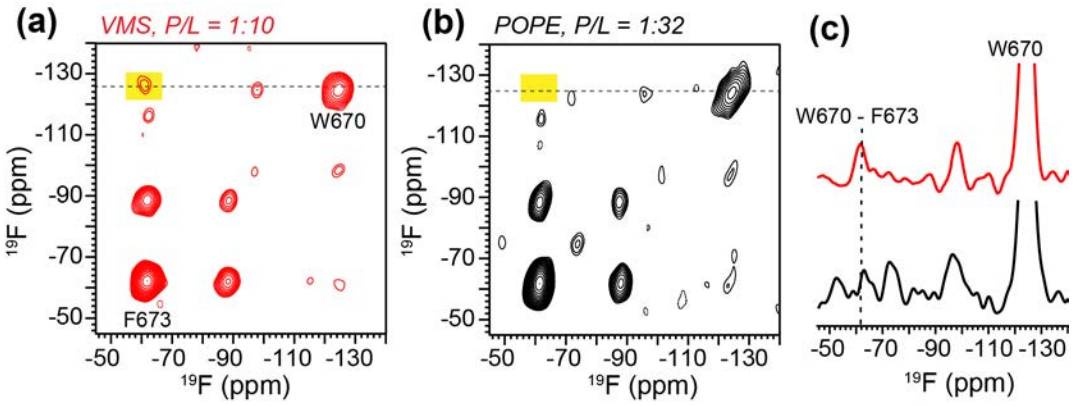

Fig. S3. 500 ms 2D ^{19}F-^{19}F spin diffusion correlation spectra of mixed fluorinated gp41 trimers. **(a)** Spectrum of mixed 5F-W670 and CF_3-F673 labeled peptides in the VMS membrane at P/L = 1:10. **(b)** Spectrum of mixed 5F-W670 and CF_3-F673 labeled peptides in the POPE membrane at P/L = 1:32. Cross peaks are highlighted in yellow. **(c)** 1D ^{19}F cross sections extracted from the 2D spectra in the W670 row. The W670-F673 cross peak is observed as expected in the VMS sample due to the high P/L ratio. In comparison, no significant cross peak is observed in the POPE spectrum at this P/L ratio.

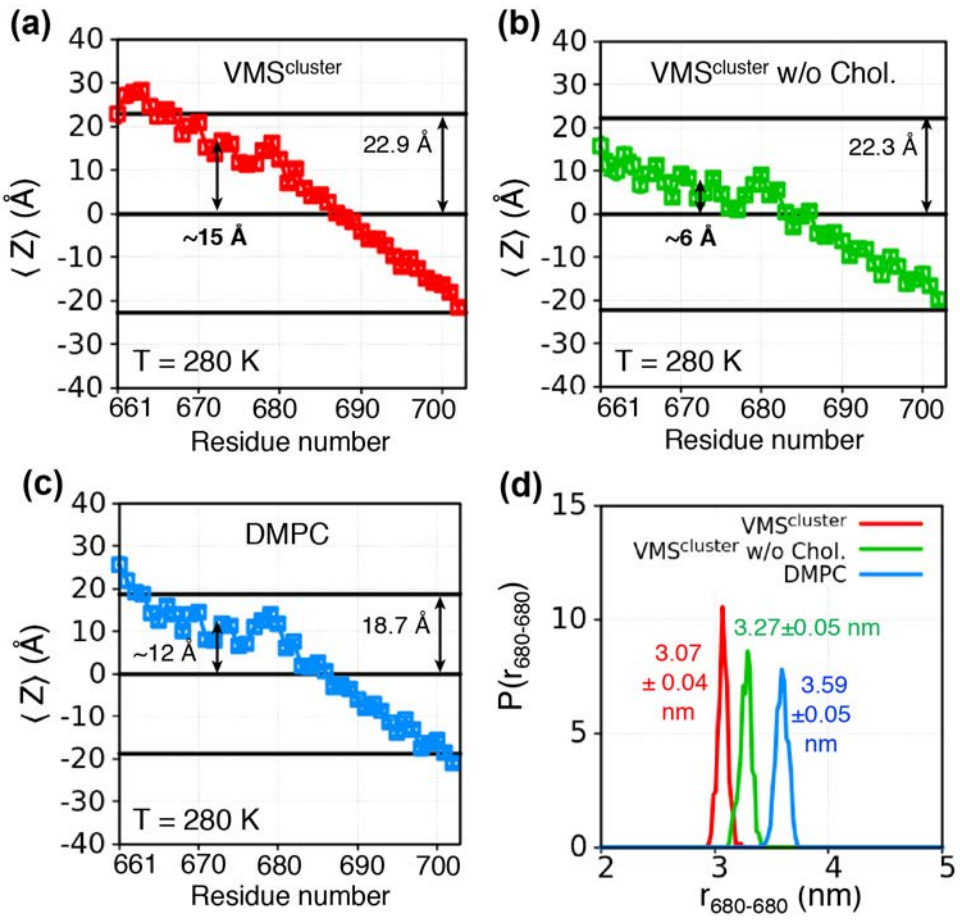

Fig. S4. All-atom simulations at 280 K to probe MPER-TMD trimer orientation, depth of insertion, and trimer-trimer association in different lipid membranes. The trends discussed in the main text based on the 303 K simulations are qualitatively reproduced at 280 K. (**a-c**) Average Z positions of gp41 residues in different membranes, with Z = 0 corresponding to the mid-plane of the bilayer. The values shown (~15, 6 and 12 Å for panels a-c) are computed for residues 670 to 675, and indicate that MPER is embedded more deeply in cholesterol-free membranes than cholesterol-containing membranes. The horizontal lines around ±20 Å indicate the average locations of the phosphorous atoms in the lipid headgroups of the three membranes. (**d**) Distributions of W680-W680 Cα atoms in adjacent MPERs in different membranes. The gp41 trimers are more tightly associated in the cholesterol-containing VMS^{cluster} membrane.

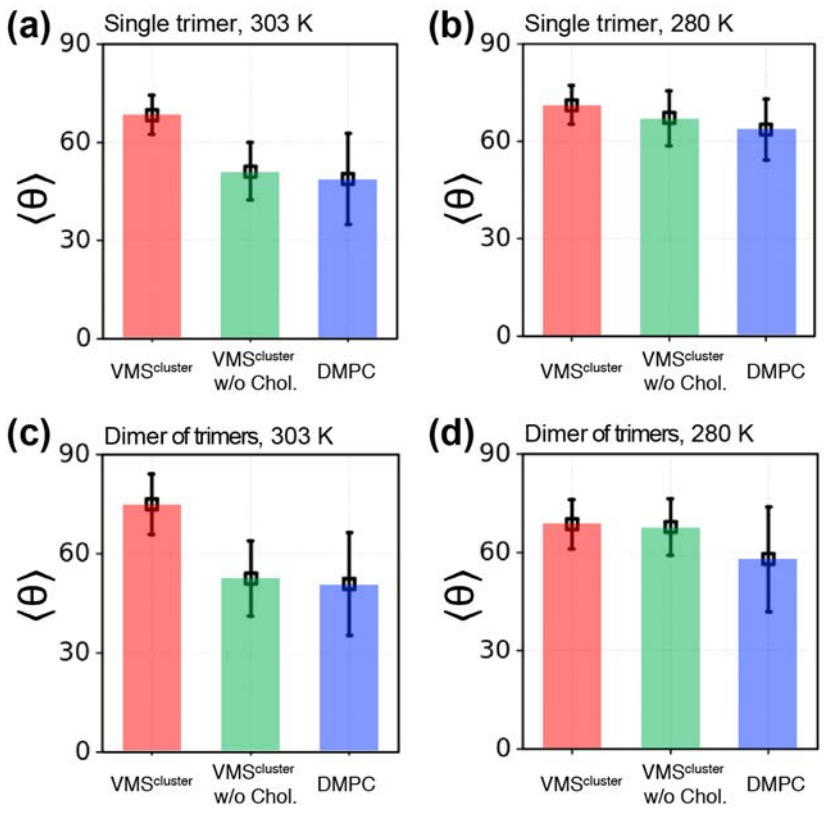

Fig. S5. Comparison of the MPER orientation in the single trimer and dimer of trimers under different conditions. The angle θ between the membrane normal and the MPER helix axis is plotted. The Cα atoms of the first and last 4 residues (L661-D664 and A677-W680) of MPER are used to define the helical axis. MPER is oriented more parallel to the membrane surface (i.e. larger θ) in the $VMS^{cluster}$ membrane than in cholesterol-free membranes in both the single trimer model and the dimer of trimers model. The angle difference is smaller at low temperature than at high temperature, in part because the DMPC membrane is in the rippled gel phase at low temperature.

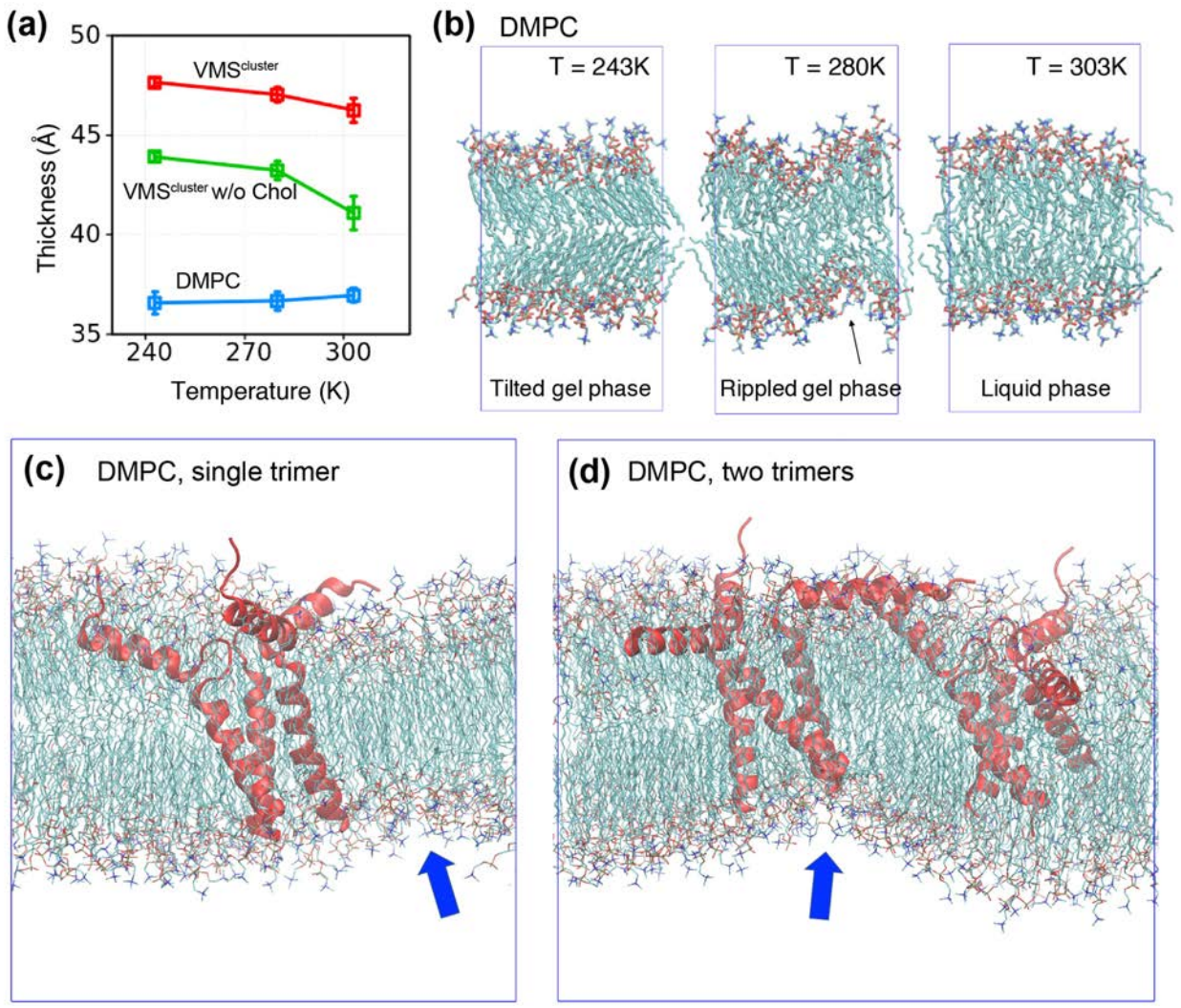

Fig. S6. Properties of the lipid membranes in the simulations at different temperatures. (**a**) Membrane thickness, defined by the average separation between phosphorus planes of the bilayer. (**b**) Different phases of DMPC membranes sampled at different temperatures. (**c-d**) At 280 K, the gel phase of DMPC is sampled in the presence of either a single gp41 trimer or a dimer of gp41 trimers. Blue arrows indicate locations that exhibit significant oscillation of membrane thickness, which impacts the MPER orientation. While the precise phase of DMPC in the solid-state NMR experiments is not known, the key trends of MPER orientation, insertion depth and trimer-trimer association are qualitatively consistent between high- and low-temperature simulations, supporting the physiological relevance of the solid-state NMR observations.

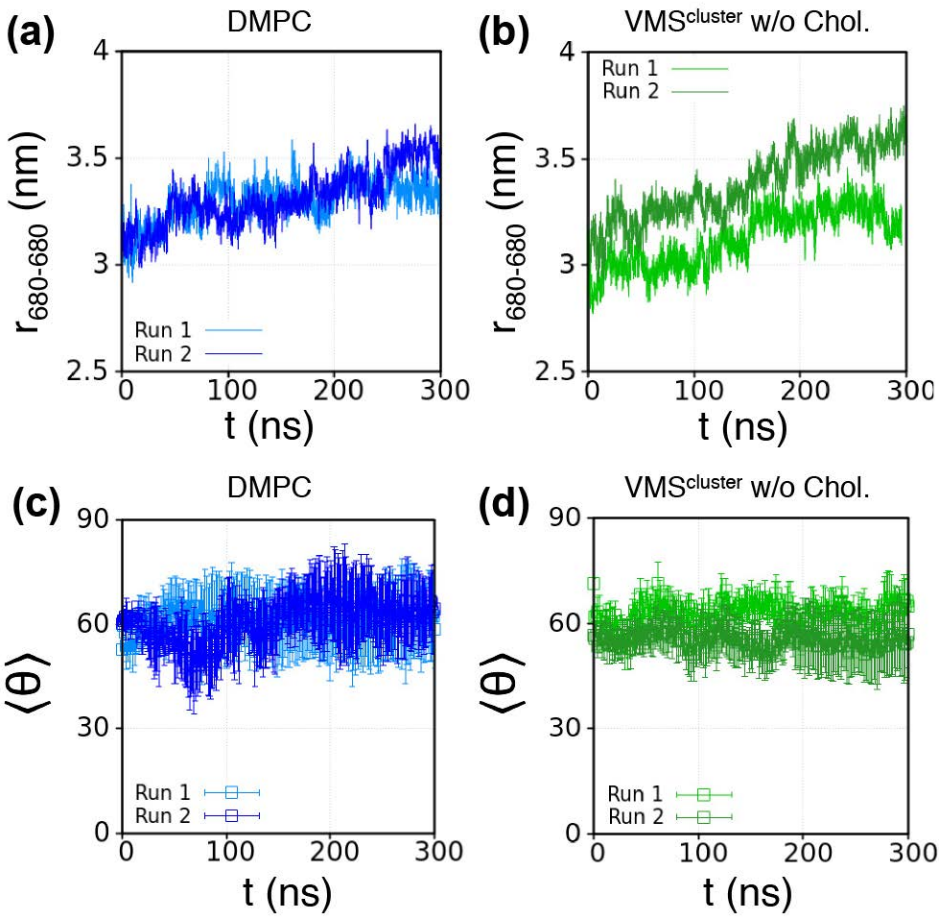

Fig. S7. Simulations of gp41 MPER-TMD dimer of trimers in lipid membranes, starting with the dimer structure found at the end of the simulation in the $VMS^{cluster}$ membrane. (**a, c**) Simulations in the DMPC membrane. (**b, d**) Simulations in the cholesterol-free $VMS^{cluster}$ membrane. (**a, b**) Distance between neighboring W680 Cα atoms in two trimers increases with time in the absence of cholesterol. (**c, d**) MPER orientation angle θ fluctuates significantly around 60° in the absence of cholesterol.

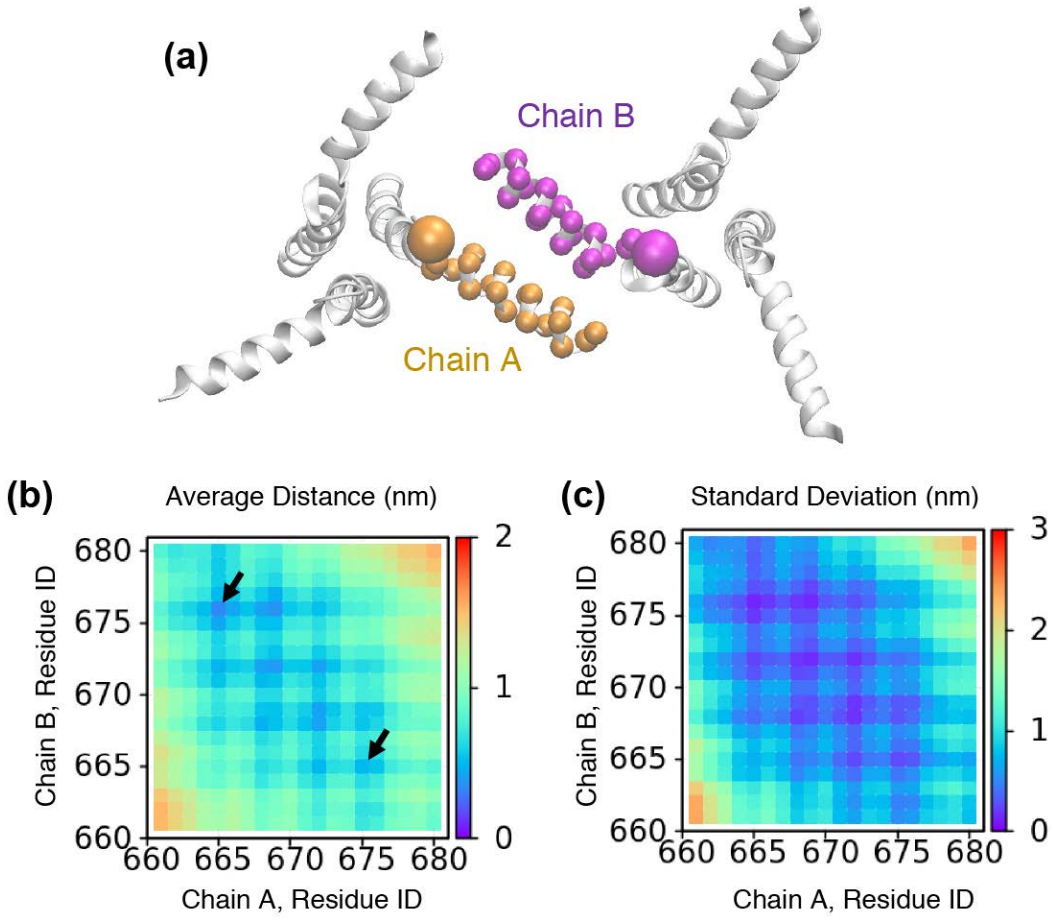

Figure S8. Distances between Cα atoms in neighboring MPER helices of two trimers from simulations of two gp41 trimers in the $VMS^{cluster}$ membrane. (**a**) Locations of Cα atoms in a snapshot; large spheres indicate the W680 Cα atoms. (**b, c**) Average and standard deviation of Cα-Cα distances. The results indicate that residues I665, D664, S668, N671 and W672 contribute predominantly to the contacts between neighboring MPER motifs.

References

[1] Jong DHD, Singh G, Bennett WFD, Arnarez C, Wassenaar TA, Schafer LV, et al. Improved Parameters for the Martini Coarse-Grained Protein Force Field. J. Chem. Theory Comput. 2013;9:687-697.

[2] Monticelli L, Kandasamy SK, Periole X, Larson RG, Tieleman DP, Marrink SJ. The MARTINI Coarse-Grained Force Field: Extension to Proteins. J. Chem. Theory Comput. 2008;4:819-834.

[3] Buzon V, Cladera J. Effect of cholesterol on the interaction of the HIV GP41 fusion peptide with model membranes. Importance of the membrane dipole potential. Biochemistry. 2006;45:15768-15775.

[4] Marrink SJ, Corradi V, Souza PCT, Ingolfsson HI, Tieleman DP, Sansom MSP. Computational Modeling of Realistic Cell Membranes. Chem. Rev. 2019;119:6184-6226.

[5] Javanainen M, Martinez-Seara H, Vattulainen I. Excessive aggregation of membrane proteins in the Martini model. PLoS One. 2017;12:e0187936.

[6] Souza PCT, Alessandri R, Barnoud J, Thallmair S, Faustino I, Grunewald F, et al. Martini 3: a general purpose force field for coarse-grained molecular dynamics. Nat. Methods. 2021;18:382-388.

[7] Majumder A, Straub JE. Addressing the Excessive Aggregation of Membrane Proteins in the MARTINI Model. J. Chem. Theory Comput. 2021;17:2513-2521.

[8] Corradi V, Mendez-Villuendaas E, Ingolfsson HI, Gu R, Siuda I, Melo MN, et al. Lipid−Protein Interactions Are Unique Fingerprints for Membrane Proteins. ACS Central Sci. 2018;4:709-717.

[9] Cino E, Borbuliak M, Hu S, Tieleman DP. Lipid distributions and transleaflet cholesterol migration near heterogeneous surfaces in asymmetric bilayers Faraday Discussions. 2021;In press.

[10] Kwon B, Lee M, Waring AJ, Hong M. Oligomeric structure and three-dimensional fold of the HIV gp41 membrane-proximal external region and transmembrane domain in phospholipid bilayers. J. Am. Chem. Soc. 2018;140:8246-8259.

[11] Jo S, Kim T, Iyer VG, Im W. CHARMM-GUI: a web-based graphical user interface for CHARMM. J. Comput. Chem. 2008;29:1859-1865.

[12] Jo S, Lim JB, Klauda JB, Im W. CHARMM-GUI Membrane Builder for mixed bilayers and its application to yeast membranes. Biophysical Journal. 2009;97:50-58.

[13] Spoel DVD, Lindahl E, Hess B, Groenhof G, Mark AE, Berendsen HJC. GROMACS: Fast, flexible, and free. J. Comp. Chem. 2005;2005:1701-1718.

[14] Berendsen HJC, Postma JPM, Gunsteren WFv, DiNola A, Haak JR. Molecular dynamics with coupling to an external bath. J. Chem. Phys. 1984;81:3684-3690.

[15] Bussi G, Donadio D, Parrinello M. Canonical sampling through velocity rescaling. J. Chem. Phys. 2007;126:014101.

[16] Parrinello M, Rahman A. Polymorphic transitions in single crystals: A new molecular dynamics method. J. Appl. Phys. 1981;52:7182-7190.